

EXPERIMENTAL INVESTIGATIONS OF NON-ROTATING
AND ROTATING TWO-DIMENSIONAL TURBULENCE

CENTRE FOR NEWFOUNDLAND STUDIES

**TOTAL OF 10 PAGES ONLY
MAY BE XEROXED**

(Without Author's Permission)

JENNIFER WELLS

**Experimental Investigations of Non-Rotating and Rotating
Two-Dimensional Turbulence**

by

© Jennifer Wells
B.Sc. (Hons.)

A thesis submitted to the
School of Graduate Studies
in partial fulfillment of the
requirements for the degree of
Master of Science.

Department of Physics and Physical Oceanography
Memorial University of Newfoundland

January 27, 2005

ST. JOHN'S

NEWFOUNDLAND





Library and
Archives Canada

Bibliothèque et
Archives Canada

Published Heritage
Branch

Direction du
Patrimoine de l'édition

0-494-06670-9

395 Wellington Street
Ottawa ON K1A 0N4
Canada

395, rue Wellington
Ottawa ON K1A 0N4
Canada

Your file *Votre référence*

ISBN:

Our file *Notre référence*

ISBN:

NOTICE:

The author has granted a non-exclusive license allowing Library and Archives Canada to reproduce, publish, archive, preserve, conserve, communicate to the public by telecommunication or on the Internet, loan, distribute and sell theses worldwide, for commercial or non-commercial purposes, in microform, paper, electronic and/or any other formats.

The author retains copyright ownership and moral rights in this thesis. Neither the thesis nor substantial extracts from it may be printed or otherwise reproduced without the author's permission.

AVIS:

L'auteur a accordé une licence non exclusive permettant à la Bibliothèque et Archives Canada de reproduire, publier, archiver, sauvegarder, conserver, transmettre au public par télécommunication ou par l'Internet, prêter, distribuer et vendre des thèses partout dans le monde, à des fins commerciales ou autres, sur support microforme, papier, électronique et/ou autres formats.

L'auteur conserve la propriété du droit d'auteur et des droits moraux qui protège cette thèse. Ni la thèse ni des extraits substantiels de celle-ci ne doivent être imprimés ou autrement reproduits sans son autorisation.

In compliance with the Canadian Privacy Act some supporting forms may have been removed from this thesis.

Conformément à la loi canadienne sur la protection de la vie privée, quelques formulaires secondaires ont été enlevés de cette thèse.

While these forms may be included in the document page count, their removal does not represent any loss of content from the thesis.

Bien que ces formulaires aient inclus dans la pagination, il n'y aura aucun contenu manquant.


Canada

Contents

Abstract	iv
Acknowledgements	vi
List of Tables	vii
List of Figures	x
1 Background	1
1.1 Introduction	1
1.2 Theory	4
1.2.1 Two-Dimensional Turbulence	4
1.2.2 Beta-Plane Approximation and Potential Vorticity	8
1.2.3 Rossby Waves and the Rhines Scale	16
1.3 Previous Numerical and Experimental Studies	23
2 Experimental Investigation of Two-Dimensional Turbulence	36
2.1 Purpose	36
2.2 Experimental Set-up and Procedure	39
2.3 Results and Discussion	41
2.4 Conclusions	52

3	Experimental Investigation of Beta-Plane Turbulence	54
3.1	Purpose	54
3.2	Experimental Set-Up and Procedure	59
3.3	Results and Discussion	63
3.4	Conclusions	83
4	References	86

Abstract

This thesis explores the behavior of decaying quasi-two-dimensional turbulent flows in non-rotating and rotating reference frames. In the non-rotating case, results from a new series of experiments on quasi-two-dimensional turbulence decaying in a rectangular container are presented. The flows are generated electromagnetically in a density stratified fluid using a regular array of permanent magnets. Particle Imaging Velocimetry is then used to determine the velocity and vorticity fields. These fields are further used to determine the global characteristics of the flow such as the energy and enstrophy. The energy spectra of the flow is found to demonstrate an upscale energy transfer and a corresponding growth of the energy-weighted mean scale. Power law exponents are obtained for both the low and high wavenumber regions of the spectra. Growth of the Reynolds number of the flow was observed during the intermediate phase of the flow evolution. In the rotating case, results from a new series of experiments on turbulent flows decaying in a thin layer of water with a free surface in a rotating circular container are presented. The flow is again generated electromagnetically and analyzed using Particle Imaging Velocimetry to obtain the velocity and vorticity fields. The experimental results demonstrate the formation of a polar vortex and jets that are perturbed by stationary Rossby waves in experiments with higher values of the beta parameter. Blocking events similar to those occurring in the Earth's atmosphere were observed in the laboratory flows. The two-dimensional

energy spectra of the flow demonstrate anisotropy in the space of the azimuthal and total wavenumbers. The one-dimensional energy spectra are characterized by a peak at the Rhines wavenumber.

Acknowledgements

I would like to take this opportunity to thank a few people without whom this work could not have been completed.

First and foremost, I would like to thank Dr. Yakov Afanassiev for his active involvement in not only this project but in my entire graduate education. His enthusiasm towards experimental physics is contagious and has helped to foster in me the same sense of enjoyment of this field. I could not have wished for a better supervisor.

I would like to thank Gary Lucas for the many things he does every day to make my life so complete. Thank you for making me smile after the bad days and for smiling with me on the good days. Your absolute confidence in me has encouraged me to always surpass my own expectations.

Finally, I would like to thank my parents, Linda and Fred Wells, whose unconditional love and support have been an amazing comfort throughout my entire life. Thank you for encouraging me to always do my best and for instilling in me the curiosity, imagination and good work ethic that has carried me through my entire education.

List of Tables

3.1	Experimental parameters for experiments on rotating turbulence. . .	62
-----	---	----

List of Figures

1.1	Schematic representation of the inverse energy and forward enstrophy cascades that exist simultaneously in a 2D homogeneous turbulent flow.	7
1.2	Schematic representation of the conservation of potential vorticity on a rotating sphere.	12
1.3	Schematic representation of the parameters used in equation 1.19. . .	13
1.4	Plot the dispersion relation for Rossby waves.	19
1.5	Plot of the boundary between turbulent and Rossby wave dominated regimes of a rotating two-dimensional turbulent flow.	22
2.1	Sketch of the experimental setup used for the experiments involving non-rotating two-dimensional turbulence.	40
2.2	Evolution of the Reynolds number of the flow for the experiments involving non-rotating turbulence.	45
2.3	Evolution of the one-dimensional energy spectrum for the experiments involving non-rotating turbulence	47
2.4	Evolution of the one-dimensional enstrophy spectrum for the experiments involving non-rotating turbulence	49
2.5	Energy-weighted mean scale l_E and enstrophy-weighted mean scale l_Z for experiments involving non-rotating turbulence.	51

2.6	Variations of the spectrum σ_E^2 and σ_Z^2 for experiments involving non-rotating turbulence.	51
3.1	Zonal bands can be easily seen in photographs of the atmospheres of Neptune, Saturn and Uranus.	55
3.2	Zonation can be clearly seen in whole disk views of Jupiter.	56
3.3	Two polar views of Jupiter	56
3.4	Schematic representation of the Jet streams that occur in the Earth's atmosphere	57
3.5	Sketch of the experimental setup used for the experiments involving rotating two-dimensional turbulence.	60
3.6	Sequence of plots that show the typical flow evolution for an experiment with a high value of β	65
3.7	500 millibar weather map of the Southern Hemisphere	67
3.8	Schematic 500 millibar weather map of North America	68
3.9	Space-time diagram of the averaged zonal velocity	69
3.10	Vorticity and velocity fields measured in two experiments with high and low values of beta	70
3.11	Radial distributions of azimuthally averaged zonal velocity and potential vorticity for two experiments with high and low values of beta.	71
3.12	700 millibar weather map showing blocked and unblocked flow over North America.	73
3.13	Zoomed velocity and potential vorticity map that demonstrates a laboratory blocking event	74
3.14	Distribution of potential vorticity along the straight line going through the centers of vortices in the dipole in Fig. 3.13	75

3.15 Two-dimensional energy spectra for two experiments with high and low values of beta	78
3.16 Evolution of the one-dimensional energy spectrum for two experiments with high and low values of beta.	79
3.17 Evolution of the energy-weighted mean scale k for total energy and for zonal energy	81
3.18 Plot of the energy-weighted mean wavenumber k_E versus isotropic Rhines wavenumber k_β	82

Chapter 1

Background

1.1 Introduction

The study of two-dimensional fluid flows is both interesting and important since coherent vortices and wakes behind solid bodies, as well as quasi-two-dimensional turbulent flows, are readily apparent in nature in atmospheric flows and density stratified flows. Quasi-two-dimensional flows (Q2D) are a useful idealization in application to many types of geophysical and astrophysical turbulence and provide a computationally accessible example of fluid turbulence. Although the evolution of a two-dimensionally turbulent flow differs greatly from its three-dimensional counterpart, it is interesting to note that one of the original driving factors that led researchers to study two-dimensional turbulence was an interest in producing numerical simulations of three-dimensional turbulence. When researchers first became interested in the study of 3D turbulence, the computing power was such that simulations of 3D turbulent flows were impossible. Even today, after all the advances that have taken place in computing power, such simulations remain extremely difficult. Thus, researchers began to focus on the more computationally accessible form of turbulence provided by two-

dimensional turbulence (Salmon, 1998). Over the years, two-dimensional turbulence has developed into an interesting field of study and has proven to be worthy of attention for its own sake due to its parallel with many geophysical flows. The vertical scale of the Earth's atmosphere and oceans are relatively small when compared to their horizontal scale with a difference of tens versus thousands of kilometers. This geometry implies that in many cases large-scale geophysical motions, such as cyclones which have a horizontal scale of a few hundred kilometers, may be adequately approximated as two-dimensional flows. Variations in vertical height of the oceans and atmosphere do of course occur, but in these situations flows are often two-dimensionalized by natural effects rather than by the depth of the fluid layer. These effects include the large-scale rotation of the Earth, and the density stratification created by such effects as sharp temperature gradients in the atmosphere and oceans and salinity gradients.

Vortex structures arise due to local forcing on a fluid and are set apart from the background fluid by their physical properties (Voropayev and Afanasyev, 1994). One of the primary vortex structures is the vortex dipole which consists of a strong jet of fluid with a system of two vortices of opposite rotational sense at its front and is characterized by a net linear momentum. The vortex structures that occur in nature tend to be long-lived and can travel great distances before they dissipate. They also appear to be quite numerous and have been observed in many satellite images where they have become visible due to the presence of an indicator such as a temperature difference, broken ice, plankton or sediments. This implies that they greatly affect our weather (or so-called "oceanic weather") since they contribute to the transport of dust, heat, salt, momentum and chemical substances (Voropayev and Afanasyev, 1994). These vortices can then interact with one another to form a turbulent flow. Additionally, when the length-scale of these vortices is large enough, spanning several degrees of latitude for example, they become influenced by the effects of the Earth's

rotation (Coriolis force). The Coriolis force greatly influences the development of these vortices and their subsequent interactions leading to the development of large-scale zonal flows such as the Jet stream and the zonal bands that are found on all of the giant planets in our solar system.

Laboratory experiments can be used to provide an effective tool for studying these Q2D flows. As such, these flows have been a subject of study in a number of recent laboratory experiments with stratified and rotating fluids or the flows in a thin layer of fluid. In all of these cases, different physical mechanisms suppress the motion in one direction and thus make the flow quasi-two-dimensional. There are many ways in which a flow can be made quasi-two-dimensional in a laboratory setting, most of which stem from the same physical principles that create these two-dimensional flows in nature. The presence of background rotation implemented by a rotating platform can be used as an aid when modelling on a smaller scale than that which is felt by the oceans and atmosphere from the earth's rotation (e.g. deVerdiere, 1980, Hide, 1968, Kloosterziel and van Heijst, 1991). Density stratification (e.g. Voropayev and Afanasyev, 1992, 1994) is another easily reproducible feature found in the oceans and atmosphere. One may also use such techniques as the employment of magnetic fields (e.g. Sommeria, 1986) or the use of thin fluid layers (e.g. Danilov and Gurarie, 2002) to study this behavior. In this study, both a two-layer density stratification as well as rotation were used separately in order to provide two-dimensionalization for the experiments presented herein.

The ease with which these two-dimensional flows can be represented in the laboratory bodes well for the advancement of knowledge in the field of two-dimensional turbulence as well as for its three dimensional counterpart. While many aspects of the evolution of two-dimensional turbulence have been explored both in the laboratory and through numerical studies, there remains many unanswered questions in this ex-

citing and complex field. As our knowledge of these turbulent processes grows so too will our understanding of many other related phenomena. This knowledge will grant us a broader grasp of our physical surroundings as well as help to shed new light on many of the mysteries involved in the formation of the structures of the galaxy and universe (Gibson, 1996).

In the following sections of this study, the characteristics of the flows of both non-rotating two-dimensional and beta-plane turbulence are discussed. Chapter 1 gives a theoretical overview of the dynamics involved in non-rotating two-dimensional turbulence and in its geophysical counterpart of rotating turbulence (*beta-plane turbulence*) as well as a brief literature review of past work done in this field. In Chapter 2, the experiments that were performed which involve non-rotating two-dimensional turbulence are discussed. An examination of the experiments that involve beta-plane turbulence is then given in Chapter 3.

1.2 Theory

1.2.1 Two-Dimensional Turbulence

There are a number of significant differences between three-dimensional turbulence and its two-dimensional counterpart. These differences can be illustrated through an examination of the 3D Navier-Stokes equation. For the velocity field $\vec{u} = (u, v, w)$, in an incompressible fluid, this equation is

$$\frac{D\vec{u}}{Dt} = -\frac{\nabla P}{\rho} + \nu \nabla^2 \vec{u} + g \quad (1.1)$$

where P is the pressure, ρ is the fluid density, ν is the kinematic viscosity, and g is the acceleration due to gravity. By taking the curl of this equation, the 3D Navier-Stokes

equation for the vorticity, $\vec{\omega} = \nabla \times \vec{u}$, in an incompressible fluid is obtained:

$$\frac{D\vec{\omega}}{Dt} = (\vec{\omega} \cdot \vec{\nabla})\vec{u} + \nu \nabla^2 \vec{u} \quad (1.2)$$

where the material derivative is $\frac{D}{Dt} = \frac{\partial}{\partial t} + (\vec{u} \cdot \vec{\nabla})$.

Equation (1.2) clearly shows that the vorticity is not conserved in 3D flows. This means that the terms on the right hand side of this equation represent the sources and sinks of vorticity in the fluid (Kundu, 2002). In equation (1.2), the term $\nu \nabla^2 \vec{u}$ is representative of the diffusion of vorticity fluctuations and is proportional to the kinematic viscosity ν of the fluid. The first term in (1.2), namely $(\vec{\omega} \cdot \vec{\nabla})\vec{u}$, is called the vortex stretching and tilting term. If we consider only the vertical component of vorticity in the 3D case, we have $(\vec{\omega} \cdot \vec{\nabla})\vec{u} = \omega_z \frac{\partial \vec{u}}{\partial z}$. This term increases the strength of a vortex if the fluid is stretched in the direction of ω . In the incompressible case, the term is proportional to the horizontal divergence $(\frac{\partial u}{\partial x} + \frac{\partial v}{\partial y})$ of the flow which implies that the strength of the vortex increases when fluid converges into the vortex thus stretching the column (Kundu, 2002). The stretching term is absent in 2D flows however, since in equation (1.2), $\vec{\omega} = \vec{\nabla} \times \vec{u} = (0, 0, \omega)$ is perpendicular to the velocity $\mathbf{u} = (u, v, 0)$ and its gradient. This absence can be illustrated by considering a 2D flow in the x-y plane. Since in the 2D case, ω is in the z direction only and $u_z = 0$, it is clear that $(\vec{\omega} \cdot \vec{\nabla})\vec{u} = \omega_z \frac{\partial \vec{u}}{\partial z} = 0$ and so $(\vec{\omega} \cdot \vec{\nabla})\vec{u}$ vanishes from equation (1.2) in the case of 2D flows.

The absence of vortex stretching in 2D flows plays a major role in the behavior of these flows. When dealing with flows that have high Reynolds numbers, as is the case in turbulent flows, the relative importance of the viscous dissipation term in equation

(1.2) can be considered to be small. This means that equation (1.2) now becomes:

$$\frac{D\vec{\omega}}{Dt} = 0, \quad (1.3)$$

which implies that for these 2D turbulent flows, the absence of dissipation leads to the conservation of vorticity for the flows.

The effect of this conservation is then to imply that any integral of the form $\int f(\omega)dA$, where $f(\omega)$ is any function of ω , will also be conserved. This means that two other important quantities of the flow will also be conserved - namely the total enstrophy

$$Z = \frac{1}{2} \int \omega^2 dA \quad (1.4)$$

and the total kinetic energy

$$E = \frac{1}{2} \int |v|^2 dA = \frac{1}{2} \int \omega \psi dA \quad (1.5)$$

where ψ represents the stream function $u = \frac{\partial \psi}{\partial y}$, $v = -\frac{\partial \psi}{\partial x}$, $\omega = -\nabla^2 \psi$.

The simultaneous conservation of energy and enstrophy in 2D flows has remarkable consequences for these flows. Through a Fourier decomposition of the velocity field, the instantaneous flow field can be represented by a spectral distribution of kinetic energy, E , over a certain range of wavenumbers k which is given by

$$E_T = \int_0^\infty E(k) dk \quad (1.6)$$

where $k = 2\pi/\lambda$. This means that physically, for domains of finite size, the smallest wavenumber k_0 in this range represents the inverse of the domain size ($k_0 \sim L^{-1}$) whereas the largest wave number k_d is the smallest scale of the flow ($k_d \sim l_d^{-1}$) where

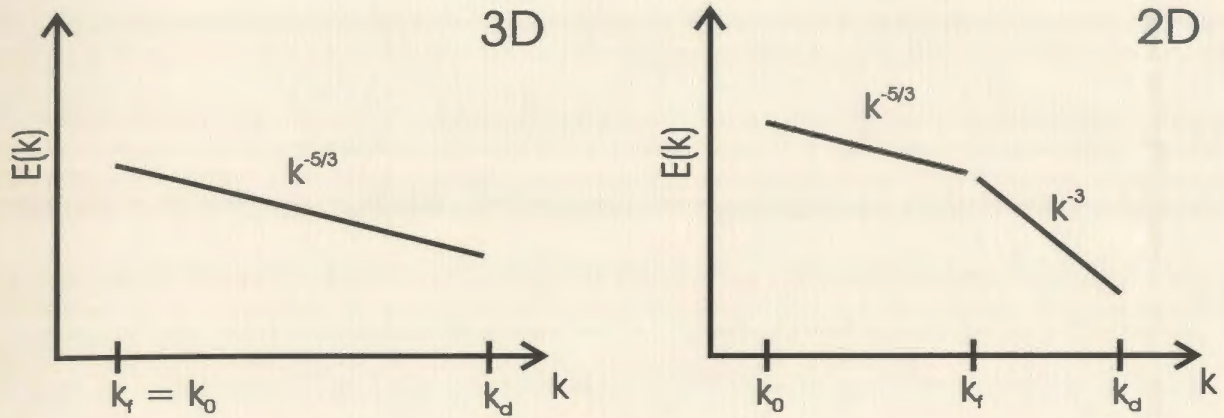


Figure 1.1: In a 2D homogeneous turbulent flow, which is continuously forced at wavenumber k_f , both an *inverse energy cascade* and a *direct enstrophy cascade* exist simultaneously as shown in this schematic representation.

l_d gives the dissipation scale.

Kolmogorov (1941) showed that at scales much larger than l_d and much smaller than L , otherwise in the range $k_0 \ll k \ll k_d$, the energy spectrum of 3D turbulence is proportional to $k^{-5/3}$ (see figure 1.1). In 3D turbulent flows, the redistribution of kinetic energy in this range results in the net transport of energy from large scales of the flow (small k) where energy is injected, towards the smallest scales (large k), where it is destroyed by dissipation. This transfer of energy is called the *energy cascade* (Batchelor, 1969). Kolmogorov then went on to show that the energy spectrum in the range is $E(k) \sim \epsilon^{2/3} k^{-5/3}$ where ϵ is the dissipation rate of the kinetic energy.

Kraichnan (1967) showed that the physical picture of 2D turbulence is quite different. He found that similar to the 3D case, the energy spectrum in 2D turbulence also satisfies $E(k) \sim \epsilon^{2/3} k^{-5/3}$ but that in the same range of k , the enstrophy spectrum $Z(k) \sim k^2 E(k)$ depends only on the constant enstrophy flux, which is equal to the constant dissipation rate of enstrophy η and the wavenumber k , giving $E(k) \sim \eta^{2/3} k^{-3}$.

This implies that in a 2D homogeneous turbulent flow, which is continuously forced at wavenumber k_f , both energy spectra exist at the same time. For $k_0 < k < k_f$, the energy spectrum is proportional to $k^{-5/3}$ and for $k_f < k < k_d$, the spectrum behaves as $E(k) \sim k^{-3}$ (see figure 1.1). The $k^{-5/3}$ range corresponds to an *inverse energy cascade* from higher to lower wavenumbers whereas the k^{-3} range yields a *direct enstrophy cascade* from lower to higher wavenumbers. Physically, this means that the energy condenses in the largest scale permitted by the boundaries of the domain, whereas enstrophy is transported to the smallest scales where it is dissipated. Batchelor (1969) also suggested this result for freely decaying 2D turbulence.

The magnitude of the enstrophy dissipation wavenumber k_d can be estimated by assuming that at the dissipation scale l_d , the advective time scale $t = \eta^{-1/3}$ is of the same order as the diffusive time scale l_d^2/ν such that

$$k_d = \frac{2\pi}{l_d} \cong \left(\frac{\eta}{\nu^3} \right)^{1/6}. \quad (1.7)$$

Strictly speaking this theory only applies to the case of *forced 2D turbulence* however computer simulations have observed the cascades in the *decaying 2D turbulent* case, where the turbulence evolves without external forcing as well (McWilliams, 1984, Brachet et al., 1986, 1988, Santangelo et al., 1989).

1.2.2 Beta-Plane Approximation and Potential Vorticity

A useful approximation that is often applied to geophysical flows is the *beta-plane approximation*. This approximation allows for a great simplification of calculations since it allows calculations involving the *Coriolis parameter* ($f = 2\Omega \sin \phi$, where Ω is the rotation rate of the sphere and ϕ is the latitude) to be performed in Cartesian rather than in full spherical coordinates. In the approximation, it is assumed that for

latitudes far from the equator on a rotating planet f can be expanded in a Taylor series about the central latitude ϕ_0 as a linear function

$$f = 2\Omega \sin \phi_0 + 2\Omega \frac{y}{R} \cos \phi_0 + \dots \quad (1.8)$$

so that

$$f \approx f_0 + \beta y. \quad (1.9)$$

Here y is the position measured from north to south and $f_0 = 2\Omega \sin \phi_0$. The *beta-parameter* β gives a measure of the rate of change of the planetary vorticity f with latitude and it is defined as

$$\beta = \left(\frac{df}{dy} \right)_{\phi_0} = \left(\frac{df}{d\phi} \frac{d\phi}{dy} \right)_{\phi_0} = \frac{2\Omega \cos \phi_0}{R} \quad (1.10)$$

where R is the radius of the sphere, $d\phi/dy = 1/R$ and $f = 2\Omega \sin \phi$. Any model that includes the β term in its definition of f is then called a β -plane model whereas a model in which there is no variation of the Coriolis parameter is called a f -plane model.

The potential vorticity is another useful quantity when describing geophysical flows and as such we will derive it here following Kundu and Cohen (2002). We begin with the equations of motion for a shallow layer of homogeneous fluid (*shallow-water model*):

$$\frac{\partial u}{\partial t} + u \frac{\partial u}{\partial x} + v \frac{\partial u}{\partial y} - fv = -g \frac{\partial \eta}{\partial x} \quad (1.11)$$

$$\frac{\partial v}{\partial t} + u \frac{\partial v}{\partial x} + v \frac{\partial v}{\partial y} + fu = -g \frac{\partial \eta}{\partial y} \quad (1.12)$$

$$\frac{\partial H}{\partial t} + \frac{\partial}{\partial x}(uH) + \frac{\partial}{\partial y}(vH) = 0. \quad (1.13)$$

Here $H(x, y, t)$ is the total depth of the fluid, η is the sea surface height above an arbitrary horizontal plane, h is the uniform undisturbed depth of the layer, x and y are taken as the eastward and northward directions respectively and u and v are the corresponding velocity components. Also, $f = f_0 + \beta y$ is the Coriolis frequency, and $H = h + \eta$.

If we differentiate equation (1.11) with respect to y and equation (1.12) with respect to x , then subtract the subsequent expressions the pressure is eliminated leaving

$$\frac{\partial}{\partial t} \left(\frac{\partial v}{\partial x} - \frac{\partial u}{\partial y} \right) + \frac{\partial}{\partial x} \left(u \frac{\partial v}{\partial x} + v \frac{\partial v}{\partial y} \right) - \frac{\partial}{\partial y} \left(u \frac{\partial u}{\partial x} - v \frac{\partial u}{\partial y} \right) + f_0 \left(\frac{\partial u}{\partial x} + \frac{\partial v}{\partial y} \right) + \beta v = 0. \quad (1.14)$$

Here f is considered a constant and has been replaced by f_0 . We then recall the relative vorticity (the vorticity measured relative to the rotating sphere)

$$\omega \equiv \frac{\partial v}{\partial x} - \frac{\partial u}{\partial y}$$

and by rearranging the nonlinear terms in equation (1.14) we are able to obtain

$$u \frac{\partial \omega}{\partial x} + v \frac{\partial \omega}{\partial y} + \left(\frac{\partial u}{\partial x} + \frac{\partial v}{\partial y} \right) \omega.$$

As such, equation (1.14) can be rewritten as

$$\frac{\partial \omega}{\partial t} + u \frac{\partial \omega}{\partial x} + v \frac{\partial \omega}{\partial y} + \left(\frac{\partial u}{\partial x} + \frac{\partial v}{\partial y} \right) (\omega + f_0) + \beta v = 0$$

and finally as

$$\frac{D\omega}{Dt} + (\omega + f_0) \left(\frac{\partial u}{\partial x} + \frac{\partial v}{\partial y} \right) + \beta v = 0. \quad (1.15)$$

where we have again used the material derivative $\frac{D}{Dt} = \frac{\partial}{\partial t} + u\frac{\partial}{\partial x} + v\frac{\partial}{\partial y}$.

By rewriting the continuity equation (equation (1.13)) as

$$\frac{DH}{Dt} + H\left(\frac{\partial u}{\partial x} + \frac{\partial v}{\partial y}\right) = 0$$

then substituting this expression into equation (1.15), we are able to eliminate the horizontal divergence ($\partial u/\partial x + \partial v/\partial y$) from equation (1.15) to obtain

$$\frac{D\omega}{Dt} = \frac{\omega + f_0}{H} \frac{DH}{Dt} - \beta v.$$

This expression can finally be written as

$$\frac{D(\omega + f)}{Dt} = \frac{\omega + f_0}{H} \frac{DH}{Dt} \quad (1.16)$$

where

$$\frac{Df}{Dt} = \frac{\partial f}{\partial t} + u\frac{\partial f}{\partial x} + v\frac{\partial f}{\partial y} = v\beta.$$

In general then we can formally define the potential vorticity as

$$q = \frac{\omega + f}{H} \quad (1.17)$$

where ω is the relative vorticity, f is the planetary vorticity and H is the thickness of the fluid measured along the vertical. Finally, from equation (1.16) the potential vorticity is a conserved quantity in the ocean's and atmosphere and as such can be written as

$$\frac{D}{Dt} \left(\frac{\omega + f}{H} \right) = 0. \quad (1.18)$$

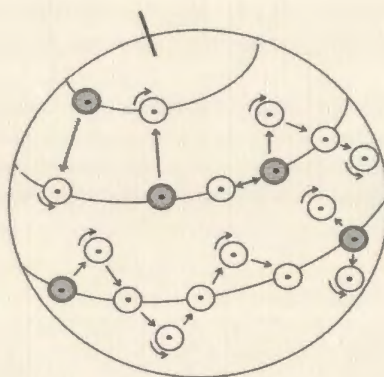


Figure 1.2: On a rotating sphere, potential vorticity can be conserved by a fluid flow through the exchange of small-scale spin for large-scale planetary spin or vice versa.

As a result of this conservation, a fluid flow (for example a rotating column of water) may exchange small-scale spin (ω) for large-scale planetary spin (f) by moving north or south on a rotating sphere. Conversely, if the water column were to make a latitudinal change a corresponding change in ω would also be required (see figure 1.2). Thus, one important consequence of the conservation of potential vorticity is that in the ocean, f tends to be much larger than ω . This means that the ratio of f/H will be constant in this case and so flow in an ocean of constant depth will be approximately zonal.

This discussion can then be extended to the case of laboratory flows. The rotating flows explored in this study were created using a technique in which an annulus with a flat bottom is filled with a fluid that has a free surface. When rotated, the surface of the fluid achieves a parabolic shape such that in the laboratory setting the value of f is a constant $f = 2\Omega$ but the total height H will vary at different radii. First, we introduce a small parameter $\delta = \frac{sr^2}{H_0}$, where $s = \Omega^2/2g$, Ω is the rotation rate of the platform, g is the gravitational constant, r is the radius and H_0 is the height of the fluid at $r = 0$ as is depicted in figure 1.3. This then allows us to write the potential

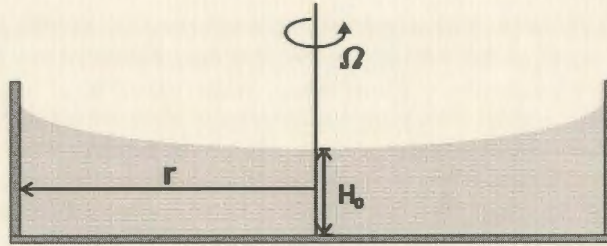


Figure 1.3: Schematic representation of the parameters used in equation 1.19.

vorticity (1.17) as

$$q = \frac{(\omega + f)}{H(1 + \delta)}$$

which we expand to

$$q = \frac{(\omega + f)(1 - \delta)}{H_0}.$$

With the assumption that the Rossby number $Ro = \omega/f \ll 1$, which in our particular case is true for intermediate and later times during the flow evolution, we can then rewrite this expression as

$$q = \frac{\omega + f}{H_0} \left(1 - \frac{sr^2}{H_0} \right). \quad (1.19)$$

As a comparison, recall that on a rotating sphere f varies with latitude as $f = 2\Omega \sin \varphi$. Introducing the angle $\alpha = \pi/2 - \varphi$, for small values of α (or equivalently for polar regions), we obtain

$$f = 2\Omega \sin \varphi = 2\Omega \cos \alpha = f_0 \left(1 - \frac{1}{2} \left(\frac{y}{R} \right)^2 \right),$$

where y is the distance in the latitudinal direction, $f_0 = 2\Omega$ and R is the radius of the sphere. The first order approximation to the actual variation of the Coriolis

parameter near the pole is known as the γ -plane approximation where $\gamma = \frac{f_0}{2R^2}$. In the laboratory system, this parameter may be introduced as $\gamma = \frac{fs}{H_0}$. The potential vorticity on the rotating sphere is then

$$q = \frac{\omega + f_0}{H_0} \left(1 - \frac{y^2}{2R^2} \right) \quad (1.20)$$

which is of similar form as the expression (1.19) for the laboratory system. Next, we formally reintroduce the beta constant such that $f = f_0 + \beta y$ where y is measured from some intermediate radius r_0 which in the case of our experiments was chosen to be one half of the radius of the container. The potential vorticity can then be rewritten as

$$q = \frac{(\omega + f)}{H_0 + s(r_0 + y)^2} \approx \frac{\omega + f - \beta y}{H_0 + sr_0^2},$$

which allows a value of β to be estimated by

$$\beta = \frac{2sr_0}{H_0 + sr_0^2}. \quad (1.21)$$

The values of s , H_0 , and β are given in Table 3.1 for the different values of Ω used in our experiments.

We then define a dimensionless beta parameter

$$\beta^* = \frac{L^2}{U} \beta$$

where U and L are the characteristic velocity and length scales of the flow. A simple dimensional analysis of the other control parameters for this system can then be used to assess the relationship between the laboratory experiments used in this study and the actual flows which occur in the Earth's atmosphere. Since the flow can be

characterized by the characteristic velocity, U and the length scale, L , of the vortices as well as the depth, H , of the fluid layer, the kinematic viscosity, ν , the Coriolis parameter, f and the beta parameter β a set of dimensionless parameters can be written:

$$Ro = \frac{U}{Lf}, \quad E = \frac{2\nu}{fH^2}, \quad Re = \frac{UL}{\nu}.$$

Here, Ro is the Rossby number, E is the Ekman number and Re is the Reynolds number. If we take typical laboratory values of $U = 0.5 \text{ cm/s}$, $L = 4 \text{ cm}$, $H = 0.5 \text{ cm}$, $f = 3 \text{ s}^{-1}$, $\nu = 0.01 \text{ cm}^2/\text{s}$ and $\beta = 0.4 \text{ cm}^{-1}\text{s}^{-1}$ we obtain

$$Ro \approx 4 \times 10^{-2}, \quad E \approx 3 \times 10^{-2}, \quad Re \approx 2 \times 10^2, \quad \beta^* \approx 1 \times 10^1.$$

This analysis shows that in the case of the laboratory experiments, the Rossby number is small meaning that the flow is geostrophic to a significant degree and the Reynolds number is large enough for nonlinear effects to be significant. The smallness of the Ekman number has important consequences for the effects of the dissipation of energy in the system and will be discussed later in chapter 3. The value of β^* is comparable with the characteristic values of this parameter for atmospheric flows. This can be seen by taking typical values for the Earth's atmosphere: $U = 10 \text{ m/s}$, $L = 6 \times 10^6 \text{ m}$ and $\beta = 4 \times 10^{-11} \text{ m}^{-1}\text{s}^{-1}$, to obtain $\beta^* \approx 100 - 200$ in this case. In the experiments which use high values of the rotation rate, with $\beta = 1 \text{ cm}^{-1}\text{s}^{-1}$ and the scale of the vortices (and zonal flows) of order $L = 5 - 10 \text{ cm}$, values of the dimensionless β^* are also found in this range. Thus this analysis indicates that the laboratory system used for these experiments can demonstrate the same dynamical phenomena as the Earth's atmosphere.

1.2.3 Rossby Waves and the Rhines Scale

An interesting consequence of the varying of the Coriolis parameter f with latitude is the existence of a type of waves called *Rossby waves* or *Planetary waves*. These waves occur quite frequently in both the Earth's atmosphere, for example as large-scale meanders of the mid-latitude jet stream, as well as in the oceans. Historically, these waves have been difficult to observe because they have a very small vertical scale of displacement (on the order of a few centimeters) relative to their horizontal scale (hundreds of kilometers). The waves are quite long-lived and can slowly travel across an entire oceanic basin. As such, they have dramatic effects on weather and climate. One such effect is the disruption as well as the intensification of western boundary currents, for example the Gulf Stream. These currents transport huge quantities of heat and so by altering even slightly the course of these currents the presence of Rossby waves can have widespread consequences.

We can take a closer look at these waves through an examination of the dispersion relation (Kundu, 2002). Recall the equation for the conservation of potential vorticity

$$\frac{D}{Dt} \left(\frac{\omega + f}{H} \right) = 0$$

which can also be written as

$$H \frac{D}{Dt} (\omega + f) - (\omega + f) \frac{DH}{Dt} = 0.$$

We expand the material derivative $\frac{D}{Dt} = \frac{\partial}{\partial t} + u \frac{\partial}{\partial x} + v \frac{\partial}{\partial y}$ and make the substitution $H = h + \eta$, where h is again the uniform undisturbed depth of the layer and η is the

surface displacement. If we then let $Df/Dt = v(df/dy) = \beta v$ this equation becomes

$$(h + \eta) \left(\frac{\partial \omega}{\partial t} + u \frac{\partial \omega}{\partial x} + v \frac{\partial \omega}{\partial y} + \beta v \right) - (\omega + f_0) \left(\frac{\partial \eta}{\partial t} + u \frac{\partial \eta}{\partial x} + v \frac{\partial \eta}{\partial y} \right) = 0. \quad (1.22)$$

The quadratic non-linear terms in equation (1.22) can now be neglected when dealing with small perturbations leaving the linearized form of the potential vorticity equation

$$h \frac{\partial \eta}{\partial t} + h\beta v - f_0 \frac{\partial \eta}{\partial t} = 0. \quad (1.23)$$

Since these waves travel so slowly, the time derivative terms in the horizontal equations of motion are an order of magnitude smaller than both the Coriolis forces and the pressure gradients. This means that the geostrophic approximation will apply to the case of Rossby waves. As such we can now make the substitution of

$$u \cong -\frac{g}{f_0} \frac{\partial \eta}{\partial y}$$

$$v \cong \frac{g}{f_0} \frac{\partial \eta}{\partial x}$$

into equation (1.23) to get the vorticity

$$\omega = \frac{g}{f_0} \left(\frac{\partial^2 \eta}{\partial x^2} + \frac{\partial^2 \eta}{\partial y^2} \right).$$

Through a final substitution of this expression for the vorticity into equation (1.23), we get

$$\frac{\partial}{\partial t} \left(\frac{\partial^2 \eta}{\partial x^2} + \frac{\partial^2 \eta}{\partial y^2} - \frac{f_0^2}{c^2} \eta \right) + \beta \frac{\partial \eta}{\partial x} = 0 \quad (1.24)$$

where $c = \sqrt{gh}$ and $R = c/f_0$ is defined as the *Rossby radius*. This equation is the quasi-geostrophic form of the linearized vorticity equation which can finally be used

to derive the dispersion relation for Rossby waves.

We now assume that equation (1.24) will have solutions of the form

$$\eta = \hat{\eta} e^{i(k_x x + k_y y - \omega t)},$$

where k_x and k_y are the east-west and north-south components respectively of the wave-vector k , such that $k^2 = k_x^2 + k_y^2$.

By substituting this value of η into equation (1.24) we are able to obtain the following expression for the dispersion relation for Rossby waves

$$\omega = -\frac{\beta k_x}{k^2 + f_0^2/c^2}. \quad (1.25)$$

This expression shows that these waves are anisotropic in the horizontal direction due to the asymmetry of the dispersion relation with respect to k_x and k_y . The waves are dispersive, that is the frequency is not directly proportional to k . Contours of constant ω are circles which can be seen from the fact that the dispersion relation (equation (1.25)) can be rearranged as

$$\left(k_x + \frac{\beta}{2\omega}\right)^2 + k_y^2 = \left(\frac{\beta}{2\omega}\right)^2 - \frac{f_0^2}{c^2}.$$

A plot of the dispersion relation for contours of constant ω is given in figure 1.4.

Next we will look at the phase and group velocities of these waves. The group velocity is defined as

$$\vec{c}_g = \vec{i} \frac{\partial \omega}{\partial k_x} + \vec{j} \frac{\partial \omega}{\partial k_y}$$

and has a direction which is perpendicular to the ω contours. We can see from the

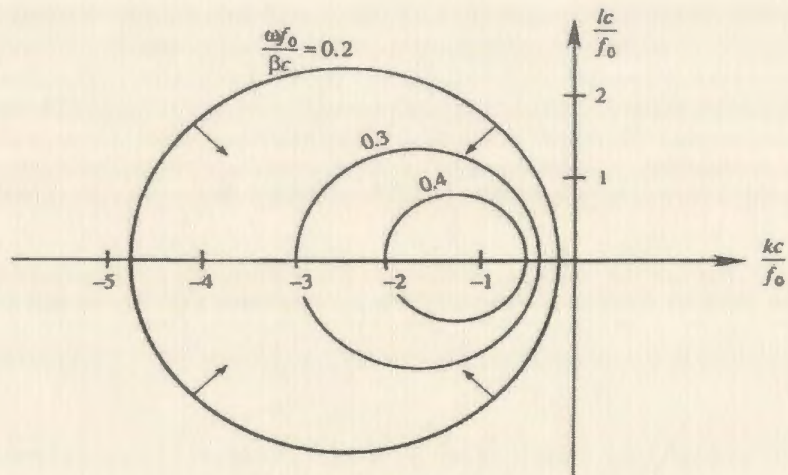


Figure 1.4: A plot of the contours of constant ω are found by plotting the dispersion relation for Rossby waves. (Kundu, 2002)

phase speed on the other hand that the waves propagate always to the west

$$c_x = \frac{\omega}{k} = -\frac{\beta}{k^2 + f_0^2/c^2}$$

with a maximum phase speed (when $k^2 = 0$) of

$$c_x \cong -\frac{\beta c^2}{f_0^2}.$$

For example, at midlatitudes we have values of $\beta = 2 \times 10^{-11} \text{ m}^{-1} \text{ s}^{-1}$, $f_0 \sim 10^{-4} \text{ s}^{-1}$, $c \sim 2 \text{ m/s}$ and a typical value of $c_x \sim 10^{-2} \text{ m/s}$ (Kundu, 2002). This means that at midlatitudes, Rossby waves move at a slow speed and therefore can take years to cross an ocean. As such, these waves affect the weather and climate to a greater extent in the lower latitudes where they move faster. Finally, it should be mentioned that the preceding analysis is not valid for latitudes very near the equator since geostrophic balance cannot be assumed for this region.

In the atmosphere, these waves are often seen on strong eastward mean flows such as the jet stream. The eastward phase speed of these waves is then given by

$$c_x = U - \frac{\beta}{k^2 + f_0^2/c^2} \quad (1.26)$$

where U is the speed of the eastward current. In this way, if the eastward current cancels the westward phase speed, $c_x = 0$, a stationary wave will be formed.

Finally, an estimate of the wavelength of these waves can be made in the following way. First, we assume that $k_y = 0$ and that the flow is barotropic so that $c = \sqrt{gh}$ is much larger than f_0 allowing us to neglect f_0^2/c^2 in equation (1.26). Since $k = 2\pi/\lambda$, this gives a wavelength for the Rossby waves of

$$\lambda = 2\pi\sqrt{\frac{U}{\beta}}.$$

In the laboratory situation where the value of c is quite large compared to f , the dispersion relation for Rossby waves will be given by the expression

$$\omega = -\frac{\beta k_x}{k^2}$$

and the phase speed by

$$c_x = \frac{\omega}{k} = \frac{\beta}{k^2}.$$

These waves create an interesting consequence in the case of beta-plane turbulence in that at some point in the flow evolution, the formation of Rossby waves will halt the energy cascade found in non-rotating two-dimensional turbulence. At this point the flow will become anisotropic and will begin to form zonal jets. For non-rotating

two-dimensional turbulence we can define an eddy turnover time scale T_U of

$$\frac{1}{T_U} = \sqrt{\int_0^k k^2 E(k) dk} \equiv Uk$$

where U is the rms velocity of the flow. T_U gives the rate at which an eddy of size k^{-1} transfers its energy to other, usually lower, wavenumbers or more physically, it is the time it takes for the eddy to be distorted by larger-scale straining motions (Salmon, 1998).

Consider the situation where $\beta \neq 0$. The influence of Rossby wave propagation on the eddy will in this case be felt on the time scale of the Rossby wave period T_w , where

$$\frac{1}{T_w} = |\omega| = \frac{\beta k_x}{k^2}.$$

Two cases can then be studied. In the first, we have $T_w < T_U$. In this case, the presence of Rossby waves alters the eddy before it can undergo significant distortion, thus rendering the energy transfer ineffective. In case two however, we have

$$\frac{\beta k_x}{k^2} < Uk \tag{1.27}$$

and β has little effect on the energy transfer to k . At its maximum, the left hand side of equation (1.27) is β/k . Thus, β is not a significant factor for any wavenumber above

$$k_\beta = \sqrt{\frac{\beta}{U}} \tag{1.28}$$

where k_β^{-1} is called the *Rhines scale*.

If the equality $\frac{\beta k_x}{k^2} = Uk$ is plotted in the (k_x, k_y) -plane the resulting curve has a dumbbell shape which is characteristically associated with beta-turbulence (see figure

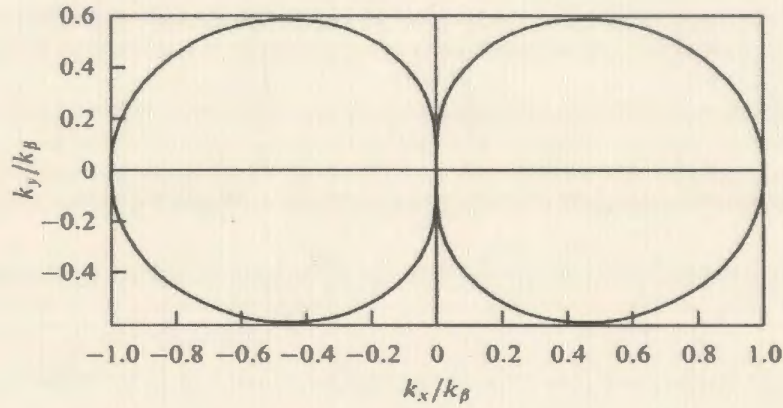


Figure 1.5: Plot of the equality $\frac{\beta k_x}{k^2} = Uk$. This plot represents the boundary between turbulent and Rossby wave dominated regimes of the flow and is a characteristic of rotating two-dimensional turbulence. (Danilov and Gurarie, 2000)

1.5). The curve reflects the nature of this turbulence in that it prevents the transfer of energy to low wavenumbers and as such represents a boundary between turbulent and Rossby waves dominated regimes. Zonal jets then form due to the proportionality of ω to k_x since energy can be transferred to a greater extent along the k_y -axis with $k_x = 0$ (Salmon, 1998). Finally, the spectral evolution of β -plane turbulence is quite different than that of non-rotating two-dimensional turbulence. In his pioneering paper, Rhines (1975) suggested that in the case of beta-plane turbulence for wavenumbers less than k_β , the turbulent energy cascade would be halted by the formation of Rossby waves. For wavenumbers above k_β he predicted a steeper energy spectrum than the $E(k) \sim k^{-5/3}$ spectrum predicted for non-rotating two-dimensional turbulence. Rhines formed his estimate of the spectrum by first estimating the fluid velocity at wavenumber k as $[2E(k)k]^{1/2}$. By equating this expression to that of the phase speed of Rossby waves, $c_p = \beta/k^2$, he was able to easily obtain an expression for the energy spectrum for

beta plane turbulence with $k > k_\beta$ of

$$E(k) = \frac{1}{2}\beta^2 k^{-5}. \quad (1.29)$$

1.3 Previous Numerical and Experimental Studies

The amount of interest that has been focused on two-dimensional turbulent flows has lead to many studies being performed in this area. Until the early 1980s however, most of the work done in this field was either theoretical or a numerical solving of the Navier-Stokes equation. Over the last few decades, a few novel techniques have been developed to study this phenomenon in the laboratory. A recent review of quasi-two-dimensional turbulence is given in Danilov and Gurarie (2000).

As mentioned in section 1.1, there are a number of ways in which a flow can be made two-dimensional. For example, in one of the pioneering experimental studies of two-dimensional turbulence, Sommeria (1986) studied forced turbulence that was generated in a relatively thin layer of conducting fluid, with a spatially and temporally varying magnetic field applied perpendicular to this layer. The experimental apparatus consisted of a square box of length 12 cm that contained a 2 cm thick layer of mercury. An electro-magnet was used to produce a uniform vertical magnetic field throughout the fluid whose upper surface was either kept free by bringing it in contact with pure nitrogen in order to avoid oxidization, or was rigid due to the formation of an oxidization layer. In order to generate the turbulent field, Sommeria embedded a series of 36 electrodes in the bottom of the box, which then acted as sources and sinks of electric current. Electric current was then provided by a d.c. power supply and the flow patterns were observed in two ways. Using the first method, small floating particles were added to the free surface of the mercury and

time exposure photographs of the flow were used to determine particle velocities and qualitative global observations. In the second case, Sommeria measured the electric potential on 11 electrodes that formed an orthogonal cross at the middle of the box. An interesting property of the electric potential is that it is directly proportional to the stream function. This allowed Sommeria to obtain a more precise determination of the flow field. Two-dimensionality was achieved in this setup through the fact that a mercury layer of this type can be divided into two regions - the lower region of the fluid, called the Hartmann layer, which is in contact with the bottom of the container and the layer of fluid which sits above it. The presence of the magnetic field should then act to damp velocity fluctuation in the vertical direction in this upper layer. Using the experimental setup, Sommeria was able to obtain, among other things, the first experimental measure of the $k^{-5/3}$ spectrum predicted for the inverse energy cascade in two-dimensional turbulence. Due to the low spatial resolution at small scales however, the setup could not be used to observe the k^{-3} spectrum predicted for the enstrophy cascade.

An alternative method that can be used to reproduce a two-dimensionally turbulent flow is the use of a thin layer of fluid like the one used by Danilov et al. (2002). In this case, the authors added a thin (2-6 mm) layer of blue vitriol to a rectangular container with horizontal dimensions of $14 \times 40 \text{ cm}^2$ and a thin bottom. In order to force the flow, the container was placed on top of a regular array of alternating magnets that had a vertical magnetization axis. A pair of electrodes was placed inside the tank on parallel walls and dc current was supplied from a power source. This method of turbulence generation is called electromagnetic forcing and it is quite frequently used in investigations of two-dimensional turbulence (e.g. Marteau et al., 1995). Since we believe that it has several advantages over its alternatives, it is the method that was used in the experiments presented herein both for non-rotating and

beta-plane turbulence. The first advantage of this method is that it allows for the creation of an approximately two-dimensional turbulent flow from the very start of the forcing. Also, there are no baroclinic effects involved with this method and the flow domain is not constrained by inner walls. The method works as follows. When current is added to the conducting fluid in a horizontal direction, the Lorentz force causes the vertical magnetic field from each magnet to create a localized horizontal force on the fluid in a direction that is perpendicular to that of the current. Since it is known that vortex dipoles and their combinations are the universal product of any localized forcing in quasi-two-dimensional systems (Voropayev and Afanasyev, 1994), the result of this forcing is the creation of a horizontal vortex dipole of zero total vorticity above each magnet. Dipolar flows have been studied in detail (e.g. Voropayev and Afanasyev, 1994, Afanasyev and Korabel, 2004) and the characteristics of the dipole can be described in terms of a single control parameter, namely the dimensionless magnitude of the momentum flux (force) that is exerted by the magnet on the fluid. The spacing between the magnets can then simply be used to give the initial length scale of the turbulent flow.

When performing the experiments, Danilov et al. (2002) allowed the current to flow through the electrodes generating the turbulent regime. After the flow was fully developed, the current was removed and the turbulence was allowed to decay until the fluid was at rest. In order to obtain measurements of the flow, the surface of the fluid was densely seeded with aluminum powder clusters and a variation of the PIV method was used. In this method, velocity fields can be obtained by imaging the flow twice in short succession, then taking the local correlations between the two images (Rutgers et al., 2001). This technique will be discussed further in section 2.2. This type of flow behaves as two-dimensional due to the fact that the horizontal scale of the flow is typically much larger than the vertical scale. In this case, the authors

observed that when using thin layers, the Reynolds number does not increase with time as was predicted by Chasnov (1997) to occur for two-dimensional turbulent flows that have an initial Reynolds number higher than some critical value. Instead, the Reynolds number was found to remain constant regardless of its initial value.

Soap films are considered the closest physical representation of two-dimensional fluids and as such are frequently used in experiments on this subject. The geometrical dimensions of the film in the direction of the plane can be extremely large when compared to the film thickness, to the extent that the film is typically 10^4 to 10^5 times wider than it is thick (Rutgers, 1999). The geometry of these films thus acts to suppress any motions perpendicular to the film, allowing any motions in the plane of the film to be considered essentially two-dimensional. There are however a few complications involved in the use of soap films to study two-dimensional turbulence. The first stems from the fact that an exact expression for the effective film viscosity cannot, as of yet, be written. Second, air drag on the film's surface can affect the governing equations for two-dimensional flows. Finally, thickness variations in the soap film may also play a role. Fortunately, the relative importance of these considerations can be reduced through a number of experimental techniques. By using thicker films (about 10 μm) the influence of both the viscosity and the effect of air drag may be greatly reduced. Also many experiments are now being performed in a vacuum chamber to eliminate the effect of air currents and air drag. Finally, a number of methods for measuring the thickness of the film (Rutgers et al., 2001, Rivera et al., 1998) exist and recent experimental set-ups (Rutgers, 1998, 1999, Wu et al., 2001, Martin et al., 1998) have been designed to create films with more uniform thickness.

Soap films have been used to shed light on many different phenomena but are most frequently used to study such flows as two-dimensional wakes behind bodies and two-dimensional turbulence. If a cylinder is inserted through a flowing soap

film a wake will be observed in the form of a simple vortex street. At low Reynolds numbers, the vortex street exhibits a two-dimensional instability (Rutgers, 1999). By placing two cylinders in the film, two stable vortex streets can be generated. Bringing the cylinders closer together allows the wakes to interact and the interaction of the vortices to be studied. These studies have shown that due to the conservation of enstrophy a repulsion will exist between the vortices with vorticity of opposite sign in the wake. In the same way, an attraction is found to be present in vortices of like rotational sign (Rutgers, 1999). To generate decaying two-dimensional turbulence in a soap film, instead of inserting a single cylinder into the film, a row of cylinders can be inserted perpendicular to the flow and the Reynolds number increased by increasing the flow rate (Rutgers, 1999, Vorobieff et al., 1999). As the film flows over the cylinders, vortices are created in their wake. These vortices all interact under the same constraint as with a single cylinder, namely that the energy and the enstrophy are conserved, and so the vortices collide and are repelled by opposite signed vortices and merge with neighbors of like sign. Experiments of this type have lead to the observation of the enstrophy cascade. The method lacks the constant forcing required to create vortices at a fixed wavenumber however and so it is unable to sustain the energy cascade. An alternative method of turbulence generation may be used to supply this forcing. By creating a soap film in a channel with rough boundaries, small vortices are created at the boundaries and then swept to the center of the channel (Rutgers, 1998, 1999). Recently, both the inverse energy cascade and forward enstrophy cascade were observed simultaneously in a flowing soap film using this method.

The first appearance of soap films as an experimental means of studying two-dimensional flows was performed by Couder in the mid 1980s (Couder, 1984, Couder et al., 1986). The apparatus used in this study consisted of a soap film stretched

onto a large stationary frame. By dragging an object through the film Couder was able to observe two-dimensional flows. Couder's technique however had a number of drawbacks. The major one being that the film had to be replaced after each test, leading to a long turnaround time between experiments.

Experiments performed by Gharib (Gharib and Derango, 1989, Beizaie and Garib, 1997) then made use of another technique that involved a flowing film moving past a stationary object. In these experiments the apparatus consisted of two rigid rails having one end connected to a reservoir of soapy water with the other end connected to a thin sheet of pure water forced from a thin slot in a metal pipe. A soap film was drawn from the reservoir, along the rails, and placed on the cascading water. The flow of the water as well as the surface tension difference between the pure water and the soap film then acted to pull the soap film forward. Obstacles that were prewetted with soap solution could be inserted into the flowing film, held stationary and the downstream wakes studied. This technique offered a significant improvement over Couder's. Since the film now flowed, as opposed to Couder's stationary film, test could be repeated without remaking the film. The flowing film could also persist for many minutes. The main drawback of this apparatus however was that the surface tension difference set a limit on the maximum speed achievable by the film, to be about 30 cm/s at a film thickness of approximately $6 \mu\text{m}$ (Rutgers, 1999).

Kellay et al. (1995) then increased the maximum speed of the films attainable in experiments to several hundred cm/s. These faster speeds were achieved through the use of an apparatus that created a vertical flowing soap film, with the motion of the soap film being driven by gravity. The apparatus consisted of two wires stretched vertically between a soap reservoir at the top and a weight submerged in a lower soap reservoir. Soapy water was allowed to leak from small perforations in the upper reservoir. The film was then drawn down between the wires to the bottom reservoir.

This new method had the advantage that the soapy water would be perpetually supplied to the upper reservoir and the film could persist for hours. Unfortunately, even though the films were quite fast, there was little control over the flow rate and film thickness. Also after the soapy water flowed through the holes it did not spread out evenly and so the flow in the film was not uniform.

The method that is currently most frequently used was created by Rutgers (1998, 1999, 2001, Martin et al., 1998) and shows a marked improvement over the other techniques as the film can persist for a very long time and it is possible to vary the film thickness while still providing a uniform flow. Rutger's setup works through the same principles as that of Kellay et al. (1995). Two wires are stretched vertically between soapy water reservoirs. In this setup however the wires meet at the upper and lower ends. At first, both wires are allowed to hang together being tied at the bottom by a weight. Soap is allowed to run down the wires through a valve that enables the control of the flow rate. Once a layer of soap coats the wires, horizontal guide wires are used to pull the vertical wires apart forming a film between them. The technique has allowed for film speeds of about 3 m/s where both the speed of the flowing film and its thickness can be easily controlled by the valve. Also, the film thickness is very uniform and can persist almost indefinitely when a pump is used to recycle water from the lower to the upper reservoir at the same rate as the flow rate from the valve. This setup has allowed for very accurate measurements of two-dimensional flows.

Flow visualization can then be performed in a number of ways. The simplest means of visualizing the flow patterns in a soap film relies on the optical interference between the front and back surfaces of the film. A change in film thickness of a quarter wavelength (approximately $0.1 \mu\text{m}$ in water) will lead to a change in the interference condition from constructive to destructive (Rutgers et al., 2001). When

viewed under a monochromatic light, these variations in film thickness then appear as dark and bright fringes. When an obstacle is inserted into the film, the interaction between the film and the object leads to the creation of thickness variations that are then advected downstream allowing the flow pattern to be visualized.

In situations where the film thickness is so large that the interference fringes become so closely spaced that they cannot be resolved by a camera, the shadowgraphing technique may be used (Rutgers et al., 2001). When using this method, light from a distant source is shone parallel to the film. As the light passes through the film, it is bent away from this parallel by the slight curvature of the film between thin and thicker regions. The bent light is then focussed into a camera. Another means of visualizing the flow is through the addition of dissolved dye molecules. One example of this technique was used by Harris and Miles (Rutgers et al., 2001) who used fluorescein dye to visualize flows. Two separate supply lines were fed into the same ejection nozzle, the first having pure soap solution and the second containing a mixture of the soap solution and the fluorescein dye. The resulting soap film thus remained dyed on only half of its surface. The downstream wakes of objects inserted into the flow at the dye line were then visualized by exposing the film to pulsed ultraviolet laser light bursts and recording the fluoresced light with a camera. Finally, the method used by Couder (Couder, 1984, Couder et al., 1986) to visualize flows in a horizontal stationary soap film involved sprinkling small particles onto the surface of the film. Photographs were taken with long exposure times such that short particle tracks became visible. More recently, seeding the films with small particles has allowed for more accurate measurements of the velocity. For example if a soap film is seeded with particles that are no thicker than the plane of the film, it is possible to obtain velocity measurements through the use of Laser Doppler Velocimetry. In this method two coherent laser beams are arranged such that they intersect the plane of the film

and create an interference pattern through which the particles pass as they follow the flow. A train of light pulses is emitted when light is scattered by the particle as it passes through the interference pattern (one pulse for each interference fringe). The particle speed can then be determined through the proportional relationship between the frequency of light pulses and the speed of the particle (Rutgers et al., 2001, Durst et al., 1981). Alternately, velocity fields can be obtained using particle imaging Velocimetry (Rutgers et al., 2001).

Density stratification can also be used to provide two-dimensionality (Marteau et al., 1995, Voropayev and Afanasyev, 1994, Maassen et al., 1999, Wells and Afanasyev, 2004). When a two-layer density stratification is employed, fluid particles are virtually unable to cross the interface between the two fluid layers. This suppresses vertical motions and as such can provide a convenient means of studying two-dimensional flows. For example, Maassen et al. (1999) studied decaying quasi- two-dimensional turbulence in a stratified flow inside a circular container. In the experiments, stratification is provided by two 10 cm thick fluid layers, the upper layer being fresh water and the lower layer having been made heavy by the addition of salt. The interface between these layers is then found to thicken slowly over a time scale of days. Outside of this layer, the authors found that three-dimensional motions show rapid decay while quasi-two-dimensional flows generated within the layer decay relatively slowly. A comb slowly towed through the fluid then provides the mechanism for generating the turbulent flows. Using this method, the authors were able to observe that the decay scenario for two-dimensional turbulence in a circular container is greatly influenced by the no-slip boundaries. The role of the net angular momentum in determining the quasi-stationary final state of the flow was also explored in this study.

Many studies on two-dimensional turbulence tend to focus on the decay process due to the fact that it has been shown (Hansen et al., 1998, McWilliams, 1990)

that the end result of this decay process is long-lived coherent vortices. Therefore, a number of theoretical and numerical studies have been directed at understanding the statistical properties of decaying two-dimensional turbulence where it was treated as an ensemble of vortices. In particular the scaling laws for different statistical characteristics of vortices in unbounded two-dimensional turbulent flows were proposed by Carnevale et al. (1991) and then tested in numerical experiments (e.g. Clercx and Nielsen, 2000) and laboratory experiments (Cardoso et al., 1994, Hansen et al., 1998).

The presence of bottom drag is believed (Danilov and Gurarie, 2000) to lead to a situation where the size of the developing coherent vortex structures do not reach their full potential. The role of bottom drag was first considered numerically by Lilly (1972) who defined a cut-off wavenumber that halts the inverse energy cascade and forces the size of the resulting vortices to remain finite. According to Lilly, this cut-off corresponds to a maximum length scale of $L_{max} \sim 0.5E^{3/2}/\epsilon$ where E is the mean kinetic energy of the flow per unit mass and ϵ is the dissipation rate due to the bottom friction. The spectral evolution of decaying two-dimensional turbulence with regular viscosity and linear bottom drag was also considered analytically by Scott (2001). In particular, it was concluded that the growth of the scale of the energy containing eddies is independent of the regular viscosity or bottom friction and therefore the upscale energy transfer remains robust to finite friction. In contrast the downscale transfer of enstrophy is limited due to a finite regular viscosity such that the enstrophy weighted scale decreases for sufficiently large Reynolds number, but increases for lower values of the Reynolds number. The behavior of these integral scales in our experiments is discussed further in later sections.

Due to its elegance in representing geophysical turbulence, a number of numerical studies have also been performed in which two-dimensional turbulent flows have been

simulated either on the Cartesian beta-plane or in spherical geometry. The evolution of the two-dimensional beta-plane energy spectrum obtained by Vallis and Maltrud (1993) demonstrated the formation of the dumbbell shaped region in the wavenumber space. As was predicted by Rhines (1975), this region is defined by the boundary between turbulent and Rossby wave regimes. These results were then confirmed using a spherical geometry by Nozawa and Yoden (1997) and Huang and Robinson (1998). The formation of anticyclonic polar vortices was first reported by Yoden and Yamada (1993) and then confirmed by Cho and Polvani (1996) who studied decaying turbulence on a sphere for a shallow water system. The results by Cho and Polvani demonstrated that inside the polar vortex, potential vorticity is well homogenized and the polar vortex is bounded by large gradients of potential vorticity. The formation of zonal jets with jet wavenumber close to the isotropic Rhines wavenumber predicted by theory is a prominent feature of numerical simulations in the area (Vallis and Maltrud, 1993).

The formation of these jets is found to be affected by a linear bottom drag since the drag is important for the stabilization of the system. This effect was studied by Manfroi and Young (1999) who on the basis of a stability analysis of a barotropic meridional flow on the beta-plane found that increasing the amount of bottom drag will directly affect both the final spacing and the number of zonal jets that form. The effects of bottom drag were further explored by Danilov and Gurarie (2002) who proposed a modification of the Rhines wavenumber that takes into account the bottom drag and who then confirmed the relevance of this number to the jet wavenumber measure in their simulations of forced turbulence on the beta-plane. Additionally, Danilov and Gurarie introduced a friction wavenumber and concluded that organized jets appear when the Rhines wavenumber exceeds the friction wavenumber.

Beta-plane flow was first studied experimentally by Whitehead (1975) who sim-

ulated the polar beta-plane by rotating a cylindrical container of water with a free surface such that the depth of the layer varies parabolically with radius. When the flow was induced locally by vertically oscillating a disc, Whitehead was able to observe a narrow eastward (prograde) jet at the latitude of forcing and a broad westward flow outside of this region. A number of other ways are now used to simulate the effect of varying the Coriolis parameter with latitude. By rapidly rotating a container with a thin layer of fluid of uniform depth, the surface will achieve a parabolic shape. Also, the effect of varying the Coriolis parameter can be achieved using varying topography by modulating the depth of the layer through the use of a container with a sloping bottom.

Forcing for these flows can then be provided in a number of ways. In some experiments a flow was induced by momentum and mass sources using a set of holes in the bottom of the tank. The fluid is pumped through one set of holes and simultaneously removed through another set (e.g. deVerdiere, 1980, Aubret et al., 2002). In the experiment by de Verdiere (1979) a zonally traveling Rossby wave which was forced by a periodic excitation of sources and sinks located in a narrow zonal region close to the outer wall of the tank was shown to excite a mean flow. Using an array of sinks and sources located along a ring in the middle of the annulus, Aubret et al. (2002) were able to observe the mixing of potential vorticity resulting in an occurrence of a zonal flow pattern with regions specified by the location of the holes. The flow was characterized by a potential vorticity gradient above the sources and sinks separating two areas of mixed potential vorticity at the inner and outer regions of the annulus. Three-dimensional small-scale motions are induced in the vicinity of the holes and may generate some mean radial motion directed from the sources to sinks that is transformed into zonal motion by the Coriolis force. Each source (sink) creates a divergence (convergence) of fluid that results in the formation of an anticyclonic

(cyclonic) vortex. In contrast to the sinks, the sources supply momentum to the fluid and therefore generate additional vorticity in the form of vortex rings. While this type of forcing provides an adequate means of inducing the flow, it also gives rise to an entire spectrum of hydrodynamic phenomena and as such cannot be easily reduced to a simple control parameter.

A second type of forcing uses the classical method of differential heating of the annulus (Hide and Mason, 1975). Rhines (1994) demonstrates a simple experiment that can easily be reproduced using a phonograph turntable. With this type of forcing, a cylindrical insert is typically placed in the center of an annulus. The inner walls are then cooled or the outer walls heated, or a combination of both. Since the cold water is denser, and thus heavier, than the warm water, the cold water sinks at the inner wall while warm water rises at the outer wall. This results in a radial flow that is directed towards the center of the container at the surface of the layer and towards the outer walls at the bottom of the container. These radial motions are then converted into zonal flows by the presence of the Coriolis force. Using this method of forcing, Bastin and Read (1998) were able to observe the formation of zonal jets as well as some stable eddy formations over a range of rotation rates.

Chapter 2

Experimental Investigation of Two-Dimensional Turbulence

2.1 Purpose

It is a well-known fact that the end result of the decay of a Q2D flow is the creation of coherent vortex structures (Maassen et al., 1999, McWilliams, 1984, Voropayev et al., 1991). These structures arise as a result of the inverse energy and forward enstrophy cascades which are characteristic of quasi-two-dimensional turbulence but are in direct opposition to the dissipative decay of three-dimensional turbulent flows. Initially, a Q2D flow will consist of a number of small vortices. Over time, these vortices will merge/pair such that two small vortices will combine to form a single vortex which contains the energy that was initially contained in the smaller vortices. This process continues until only a few large vortices remain. In this way the energy that was initially contained in the small-scale vortices is transferred through the process of vortex mergers to the large-scale. Spectrally, this process of vortex pairing is represented by the simultaneous inverse energy cascade ($E(k) \sim k^{-5/3}$) and forward

enstrophy cascade ($E(k) \sim k^{-3}$) which was described in Section 1.2.1. The end result of this process is the formation of coherent vortex structures. These structures share many characteristics which lead to their visibility and importance to geophysical fluid flows.

One of these important features is the stability of coherent vortex structures with respect to small perturbations. This stability gives the vortices the ability to persist over relatively long time scales without being destroyed. The vortices are also only weakly dissipative for most of their lifetime and so these structures can travel for significant distances and provide a means of transporting material properties (McWilliams and Weiss, 1994). Finally, coherent vortices tend to have large spatial separations, or in other words are typically isolated structures, and thus they interact only weakly with each other. This is fortunate since even though interactions are rare, these events usually mean the transformation or even destruction of the structures (McWilliams, 1984).

These coherent structures are frequently seen in nature both at the large and small scales. Velocity shear, particularly when it occurs in a narrow layer, is often unstable which may result in the creation of isolated vortices (McWilliams and Weiss, 1994). These vortices are circularly symmetric about an axis that is perpendicular to both the mean velocity and the velocity gradient. This result lends itself to the case of atmospheric flow past mountainous island topography which leads to vortex formation in stratus cloud patterns. It also applies to oceanic flow past undersea mountain topography leading to vortex formation visible in the sea-surface surfactant patterns. The result may also be applied to unstable free-shear layers which is the cause of many sea-surface temperature patterns. Coherent structures called buoyant plumes which occur in cumulus clouds in the atmosphere and as oceanic chimneys are a result of the dynamics of buoyancy-driven planetary boundary layers. The process

of adjustment, whereby a local density or momentum anomaly creates a vortical circulation which in turn causes Coriolis or centrifugal forces to balance the pressure gradient, produces many types of anticyclonic coherent vortices in the ocean interior (McWilliams and Weiss, 1994). These vortices can then be detected by their locally anomalous chemical concentrations and can persist for long periods of time as well as travel great distances. Mushroom vortices, or dipoles, can also be caused by the adjustment of local momentum impulses and are often seen in sea surface temperature and color images. Baroclinic instability of the vertical shear of horizontal velocity in a stratified fluid with a large enough scale to be affected by the Earth's rotation can also produce coherent vortices. Vortices produced in this manner include cyclones of the extra-tropical atmosphere and vortices found in the ocean's marginal ice zones. The long-lived vortices in the atmospheres of gas giant planets, such as Jupiter's Great Red Spot and Neptune's Great Dark Spot, provide distinct examples of coherent vortex structures. The polar vortices found in the Earth's stratosphere can also be considered coherent structures. The Earth's spherical shape constrains the vortex's behavior so that mixing between the vortex and its surroundings is limited to a narrow zonal band and there is relatively little matter exchanged. This may also be the cause of decreased ozone concentrations in these regions.

The purpose of this study is to provide experimental confirmation of a few of the key features that have been predicted for a non-rotating two-dimensional flow. The main goal of this work is to examine the spectral features of decaying two-dimensional non-rotating turbulence by performing high resolution velocity measurements in a system with controlled forcing. This analysis should provide an experimental example of such features as the inverse energy cascade and the enstrophy cascade as well as to demonstrate experimentally the predicted growth of the Reynolds number of the flow.

2.2 Experimental Set-up and Procedure

A square container of dimensions 29 x 29 cm was used in the series of 5 experiments in which the spectral characteristics of decaying turbulence in the non-rotating case were investigated. An array of 14 x 14 magnets of alternating polarity were used in these experiments. Each magnet had a diameter of 1.4 cm and generated a magnetic field with a vertical component of approximately 0.09 T. The flow was forced electromagnetically by imposing an electric current of magnitude 3A in the horizontal direction between two parallel graphite electrodes. The interaction of the magnetic field above each magnet and the electric current produced a localized horizontal force on the fluid in a direction perpendicular to both of these fields. Since the universal result of a localized force on a fluid is the generation of a vortex dipole, the combined result of the forcing in this case is initially an array of closely packed dipoles that share vortices with their neighbors. Due to the nonlinearity of the system, the vortices do not remain in a regular lattice, but instead they are in motion creating a typical 2D turbulent field. The container was filled with two layers of water, each of 0.5 cm depth, which had salt concentrations of 40 g/L and 250 g/L.

In order to perform an analysis of the resultant flows, a method called Particle Imaging Velocimetry (PIV) was used to generate horizontal velocity fields of the flow. A description of the method and general technique is given by Fincham and Spedding (1997) and Pawlak and Armi (1998). This method allows one to generate velocity fields from videos of the flows by tracking the motion of groups of tracer particles in the flow. The first step in this process is to add a tracer to the flow that is to be analyzed. This tracer must be able to follow the flow without interfering with it and must be sufficiently set apart from the background such that the motion of the

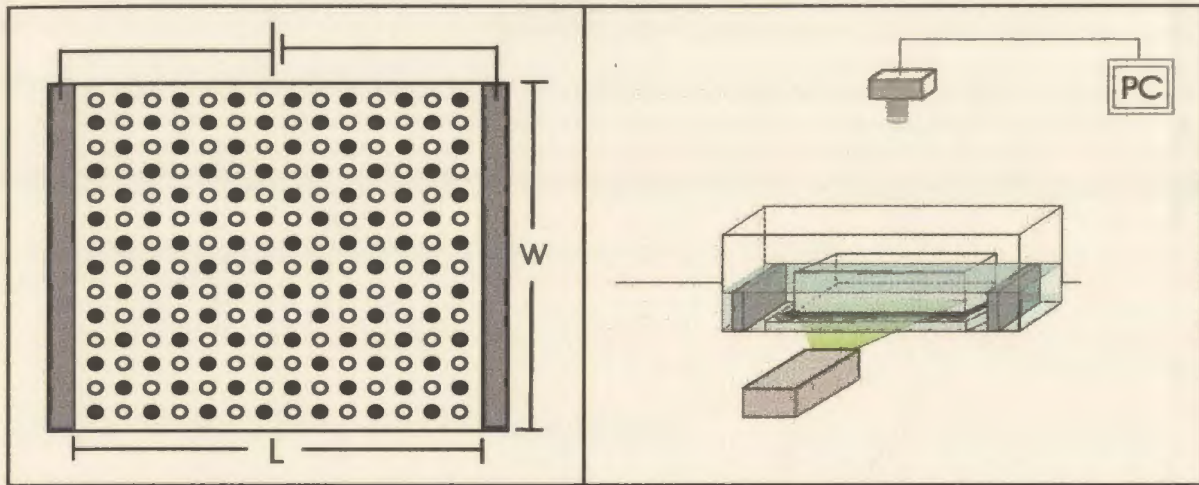


Figure 2.1: Sketch of the experimental setup used for the experiments involving non-rotating two-dimensional turbulence. (a) top view (b) side view.

tracer can be recorded. The seeding particles used in the experiments on non-rotating turbulence were polyamid spheres of mean diameter $50 \mu m$, with a neutral density that allowed them to float on the interface of the two-layer stratification. The particles were then made visible by illuminating the fluid with a sheet of light from an Argon Ion laser at the mid-height of the layer.

The next step in the PIV process is to record a video of the flow in order to obtain the local displacement of particles between successive frames of the video. Top images of the flow were taken with a digital video camera with an array resolution of up to 1288×1032 pixels. The typical spatial resolution of the images was 36 pixels/cm. Video frames were recorded directly into computer memory. Using PIV, the local displacements of particles were tracked between frames by examining the local displacement of groups of particles in small regions in the image. The displacement of the particle groups were then determined and used to calculate instantaneous velocity fields for the flow.

The commercial software MathWorks Matlab was used to both generate the velocity fields as well as to carry out further processing of these fields. Processing of the data was performed on workstations with double Alpha processors where successive images with a frame rate of 7.3 fps were used to obtain 3.7 velocity fields per second with the velocity fields having a resolution of 99 x 99 vectors.

2.3 Results and Discussion

As was mentioned in section 1.2.2 an important non-dimensional parameter is Reynolds number which represents the ratio of inertia force to viscous force and gives a measure of the non-linearity of the system. For the case of the work done here we can define two values for the Reynolds number. The global Reynolds number,

$$Re_g \equiv \frac{LU}{\nu},$$

gives a measure of the relative importance of inertia force to viscosity on the scale of the container. In the same way, a local Reynolds number,

$$Re \equiv \frac{lU}{\nu},$$

can then be defined to characterize the importance on the scale of an elementary vortex. Here U is the rms velocity of the flow, L is the length of the container, and $l = \frac{U}{\Omega}$ is the length scale of an elementary vortex with rms vorticity Ω . Other authors usually define this local Reynolds number according to either the radius or the diameter of the vortex. This is because if an elementary vortex of radius R is in solid body rotation, R can be defined from $U \equiv \frac{\Omega}{2}R$ which is the linear velocity at

the vortex's periphery. The local Reynolds number used here was chosen to match the one used by Chasnov (1997) for the purpose of comparison.

In laboratory situations, the contribution of bottom drag as a means of dissipation must be considered in addition to that of viscosity. In fact, the evolution of a laboratory flow will be constrained by whichever of these factors dominate. This means that one obstacle which must be overcome when studying two-dimensional turbulent flows in the laboratory is the effect of bottom friction.

One method of accomplishing this goal is to perform the experiments in a soap film where it is possible to decrease the equivalent contribution of air drag through a reduction of air pressure. The production of quasi-two-dimensional flows in a thin layer of fluid however is technically easier to accomplish. The most straightforward means of reducing bottom drag in this case is to simply increase the depth of the fluid layer. This in itself poses a problem however, in that the fluid depth must not be so great as to exclude two-dimensionality. Therefore, the depth of the layer is especially significant at early times in the flow evolution when the flow is most intense and the horizontal scale of the flow, or the width of the constituent vortices, is comparable to that of the depth. In the part of this study that explores beta-turbulence, rotation was used to offset the three-dimensional effects introduced by the depth of the fluid. For the experiments which explore non-rotating turbulence, a two-layer stratification was used to accomplish the same task. Differences in salinity often arise in the ocean, and temperature differences are common in both the atmosphere and oceans. Consequently, situations often arise where in the absence of mixing a density difference, or density stratification, is present between two regions of fluid and a geophysical flow can behave as if it is almost, or quasi, two-dimensional. A study of the use of stratification as a means to suppress three-dimensional motions in experimental flows was made by Paret et al. (1997) where it was found that these

flows might be treated as two-dimensional after a short transient state.

The reduction of bottom drag in these experiments does not greatly affect the form of the energy spectrum $E(k)$. Scott (2001) determined that neither regular viscosity nor bottom drag affect the growth scale of the energy containing eddies and consequently the upscale energy transfer remains unaffected. The downscale transfer of enstrophy however is affected by regular viscosity in that the enstrophy weighted scale decreases for sufficiently large Reynolds numbers but increases for lower Reynolds numbers. The bottom drag significantly affects the temporal evolution of the Reynolds number as well. Chasnov (1997) predicted that in the case of a decaying non-rotating two-dimensional turbulent flow, if the initial Reynolds number is greater than some critical value, the Reynolds number will increase with time. The value of this critical Reynolds number Re_c was determined numerically by Chasnov (1997) to be $Re_c = 15.73$. This prediction has been previously confirmed in experiments in a soap film (Martin et al., 1998) but not in those using a thin layer of fluid (e.g. Danilov and Gurarie, 2002) where the Reynolds number remained constant with time. In the experiments with a thin layer of fluid, the authors determined that in their experiments, ordinary viscosity could only account for one-fourth of the total energy decay rate initially and an even lower value at later times in the flow evolution. It is obvious then that bottom friction governed the dissipation in these experiments.

The contribution by bottom friction for the experiments reported herein can be estimated by examining the decay rate of the total energy of our flow in the following way. Bottom friction is commonly parameterized by a linear term in the vorticity equation

$$\frac{D\omega}{Dt} = -\lambda\omega + \nu\nabla^2\omega.$$

Here, ω is the vorticity and ν is the kinematic viscosity. λ is the linear drag coefficient

which causes an exponential decay of energy.

Danilov and Gurarie(2002) found that the mean exponent of energy decay due only to bottom friction can be estimated as

$$2\lambda = \frac{d\ln(E)}{dt} - 2\nu \frac{Z}{E} \quad (2.1)$$

where $E = U^2$ is the energy per unit mass and $Z = \Omega^2/2$ is the enstrophy per unit mass. The term $-2\nu Z/E$ in equation (2.1) represents the contribution made by ordinary viscosity to the decay rate. This term is found to vary during the experiments while the total rate of energy decay remains approximately constant. The typical decay rate of the total energy in our experiments involving non-rotating turbulence was measured during an intermediate time of 10 s after forcing ceased and was found to have a value of $d(\ln E)/dt = -0.024 \text{ s}^{-1}$. For the experiments involving non-rotating turbulence the value for the linear drag coefficient was estimated to be $2\lambda = 0.012 \text{ s}^{-1}$ for intermediate times in the flow evolution but then increased to 0.017 s^{-1} towards the end of the experiments. Therefore, in these experiments, both the bottom friction and the ordinary viscosity were found to contribute equally to the total energy decay. In our experiments, initial values for the Reynolds numbers were estimated to vary between $Re_g = 650 - 1000$ and $Re = 15 - 20$. The values, which were estimated immediately after the forcing ceased, are close to the critical value that was predicted by Chasnov (1997).

The local Reynolds number of the flow,

$$Re = \frac{lU}{\nu} = \frac{E}{\Omega\nu}$$

was then plotted as a function of time for our experiments with non-rotating tur-

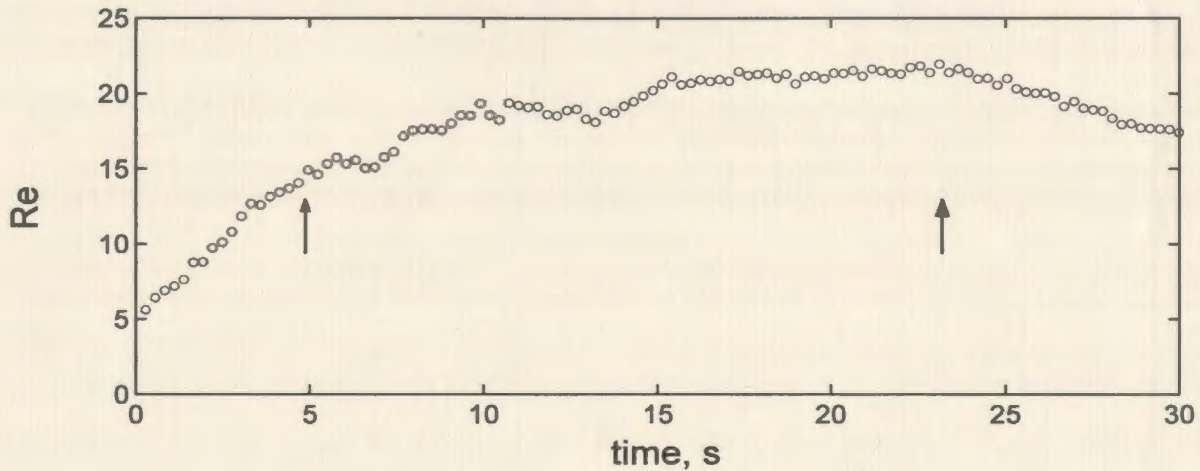


Figure 2.2: Evolution of the Reynolds number of the flow for the experiments involving non-rotating turbulence. Arrows indicate the intermediate range where Re is growing after the end of the forcing ($t = 5s$).

bulence (figure 2.2). In this plot we see the growth of the Reynolds number as was predicted by the fact that although close to Re_c , our initial value for the Reynolds number was above this critical value. In addition, the growth of the Reynolds number in these experiments can be used as confirmation that the regime of the flow corresponds to that of two-dimensional turbulence. It is also interesting that in similar experiments performed by Danilov et al. (2002) this growth was not observed even though the initial value of the Reynolds number was higher than those used in this study. This implies that the relative magnitude of bottom friction compared to that of the regular viscosity significantly affects the regime of the flow.

Now, we take a closer look at the spectral characteristics of the non-rotating two-dimensional turbulence. For each component of the velocity (v_x, v_y), the two-dimensional power spectra $S_{xx} = v_{nm}v_{nm}^*$ and $S_{yy} = v_{nm}v_{nm}^*$ in wavenumber space (n, m) were calculated. Here, time averaging was performed at intervals of 1 s. Then, the one-dimensional energy spectrum was obtained by integrating over the angle ϕ in

wavenumber space. This one-dimensional energy spectrum is given by

$$E(k) = \frac{1}{2} \frac{k}{(2\pi)^2} \int_0^{2\pi} (S_{xx} + S_{yy}) d\phi$$

where $k = (n^2 + m^2)^{1/2}$ is the radial wavenumber.

A typical energy spectrum for the experiments with non-rotating turbulence is given for different times in figure 2.3. There are a few features worth noting in the energy spectrum for these experiments. The first is the peak that occurs at wavenumber $k \approx 10$. This energy peak represents the scale of energy injection since it occurs at approximately the forcing wavenumber $k_f = (n^2 + m^2)^{1/2} = 7\sqrt{2}$, where we have used an array of 14×14 magnets of alternating polarities to force the flow. A second feature that is worth mentioning is the peak that occurs at half of the forcing wavenumber $k_1 = k_f/2$ due to the pairing of the original vortices of like sign and the corresponding transfer of energy from the original peak to the subharmonic peak. It is interesting to note that this transfer occurs through the decrease of the original peak with a corresponding increase in the subharmonic peak as opposed to a continuous shift of the original peak towards lower wavenumbers. To a lesser extent, further pairing of the vortices can be seen to occur at $k_2 = k_1/2$ in the energy spectrum. Finally, the shape of the energy spectrum for these experiments has the form $E(k) \sim k^m$, where $m = -3.0 \pm 0.15$ for the high wavenumber part of the spectra and $m \cong 1$ for the low wavenumber part of the spectra. The value of $m = -3.0 \pm 0.15$ which was found for the high wavenumber part of the spectra is in agreement with classical theory. The value of $m \cong 1$ which was found for the lower wavenumber region grows more slowly than the scaling regime of $m = 3$ which was predicted by Lesieur (1991) but is however in agreement with the results of experiments in soap

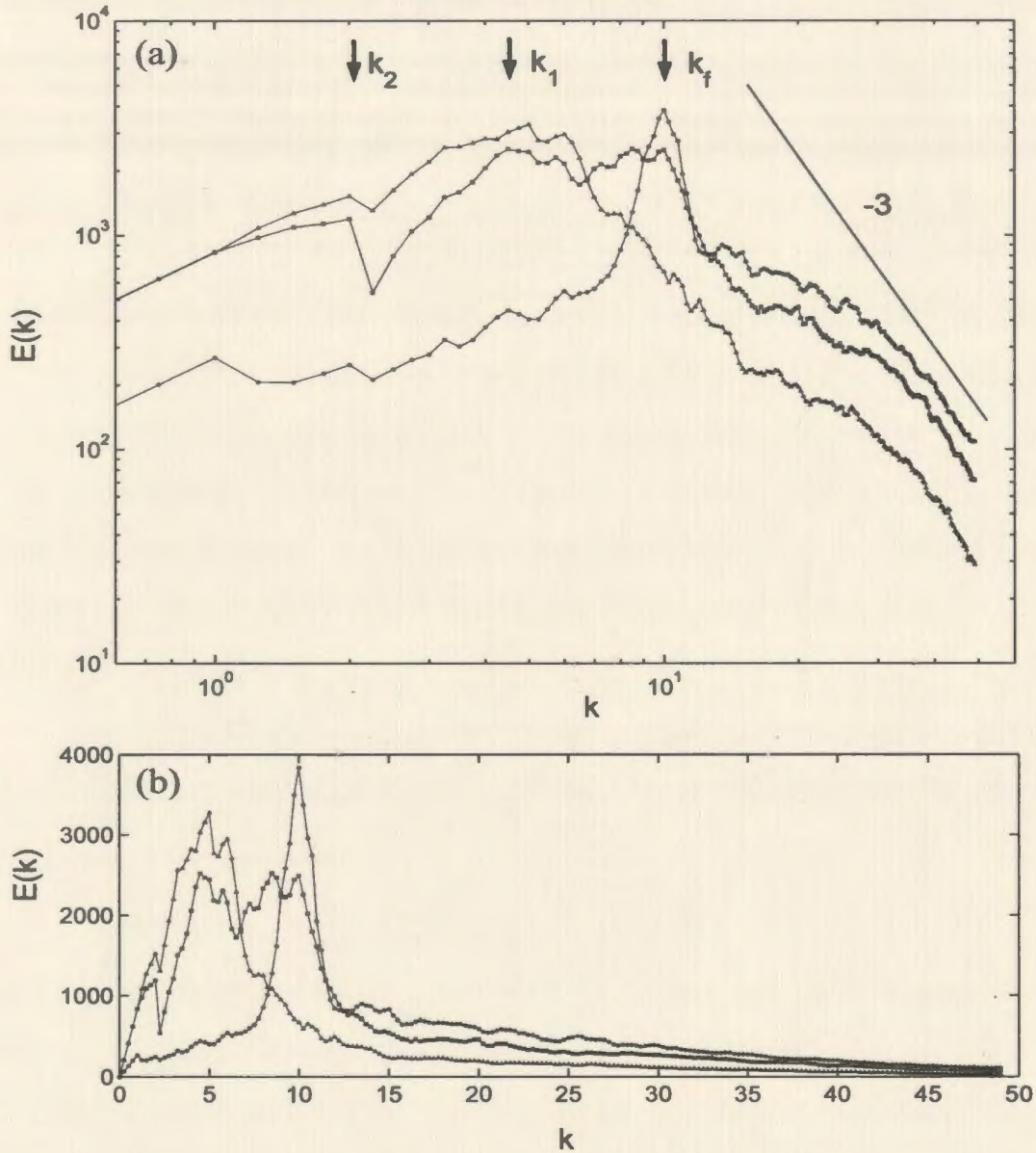


Figure 2.3: Evolution of the one-dimensional energy spectrum for the experiments involving non-rotating turbulence in logarithmic (a) and in linear (b) coordinates: $t = 8.6s$ (circles), $t = 14s$ (squares), $t = 20s$ (triangles). Forcing stops at $t = 5s$ in this series of experiments. The forcing wavenumber and two subharmonic wavenumbers that occur due to pairing of vortices are indicated by arrows.

films (Martin et al., 1998).

Next, the one-dimensional enstrophy spectrum for the non-rotating turbulence was calculated according to the same method used to calculate the energy spectrum and was then plotted (see figure 2.4). The peaks that occur in the enstrophy spectrum are similar to those that were seen in the energy spectrum. If we consider a time interval that corresponds to the intermediate asymptotic regime during which the Reynolds number grows, the enstrophy spectrum shows a peak at the forcing wavenumber for an initial time as well as a peak at the subharmonic wavenumber at the end of the time interval. In contrast to the energy spectrum however, at intermediate times, the peak in enstrophy at the forcing wavenumber does not shift towards the subharmonic wavenumber. In addition, this peak spreads symmetrically to higher and lower wavenumbers.

In order to more fully examine the behavior of the spectral evolution of the flow we can study the moments of the energy spectrum. Scott (2001) defines the n^{th} moment as

$$M_n(t) = \int_0^\infty k^n E(k, t) dk \quad (2.2)$$

such that M_0 corresponds to the total energy of the flow and M_2 to its total enstrophy. These moments can then be used to define additional integral characteristics of the flow. The energy-weighted mean wavenumber k_E provides a measure of the energy containing scale and is defined as

$$k_E(t) = \frac{\int_0^\infty k E(k, t) dk}{\int_0^\infty E(k, t) dk} = \frac{M_1}{M_0}. \quad (2.3)$$

According to Scott (2001) this wavenumber should decrease with time regardless of the values of the ordinary viscosity or the linear bottom friction coefficient corresponding

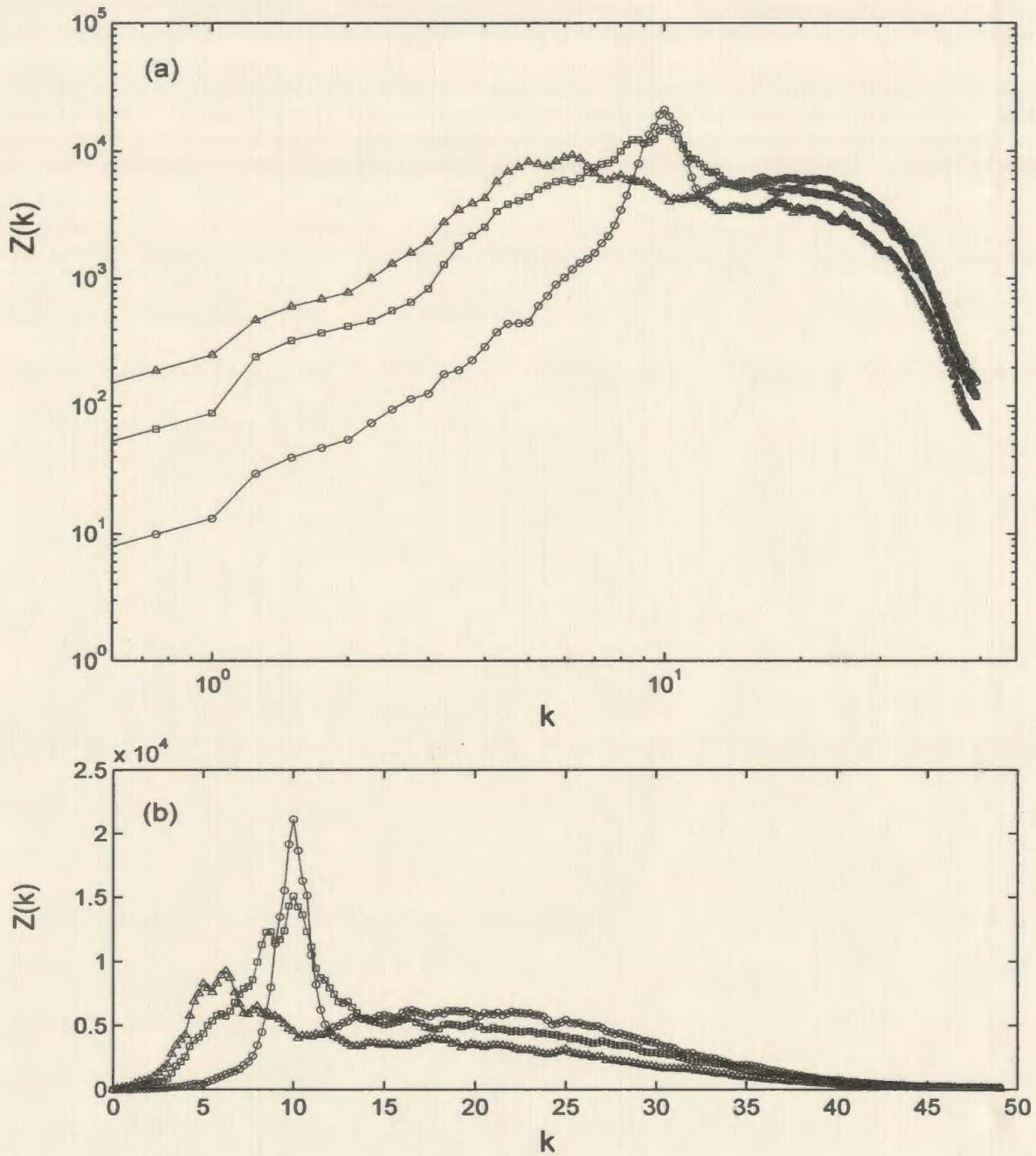


Figure 2.4: Evolution of the one-dimensional enstrophy spectrum for the experiments involving non-rotating turbulence in logarithmic (a) and in linear (b) coordinates: $t = 8.6s$ (circles), $t = 14s$ (squares), $t = 20s$, (triangles). Forcing stops at $t = 5s$ in this series of experiments.

to an upscale energy transfer. Next, we have the enstrophy-weighted mean scale l_Z which provides a measure of the enstrophy containing scales and is defined as

$$l_Z(t) = \frac{\int_0^\infty k^{-1} Z(k, t) dk}{\int_0^\infty Z(k, t) dk} = \frac{M_1}{M_2}.$$

The behavior of this value is expected to depend on the Reynolds number such that it decreases for sufficiently large Reynolds number corresponding to the downscale transfer of enstrophy. Finally, the variance of the energy spectrum σ_E^2 and that of the enstrophy spectrum σ_Z^2 are given by

$$\sigma_E^2(t) = \frac{M_2}{M_0} - k_E^2$$

and

$$\sigma_Z^2(t) = \frac{M_0}{M_2} - l_Z^2.$$

The growth of these variances should then correspond to spreading in wavenumber space.

Numerical integration of the appropriate moments of the one-dimensional energy spectra was then performed for the experiments involving non-rotating turbulence in order to estimate the preceding integral characteristics for our experiments. The typical temporal evolutions of l_E , l_Z , σ_E^2 and σ_Z^2 for the experiments involving non-rotating turbulence were then plotted in figures 2.5 and 2.6. Here l_E is the energy-weighted mean scale given by $l_E = 1/k_E$. From figure 2.5 we can see that during these experiments l_E increases linearly from a value of 0.065 to about twice that value while l_Z remains approximately constant. Physically, the initial value of $l_E = 0.065$ ($k = 15$) corresponds approximately to a scale of 2.9 cm which in turn is equal to the distance

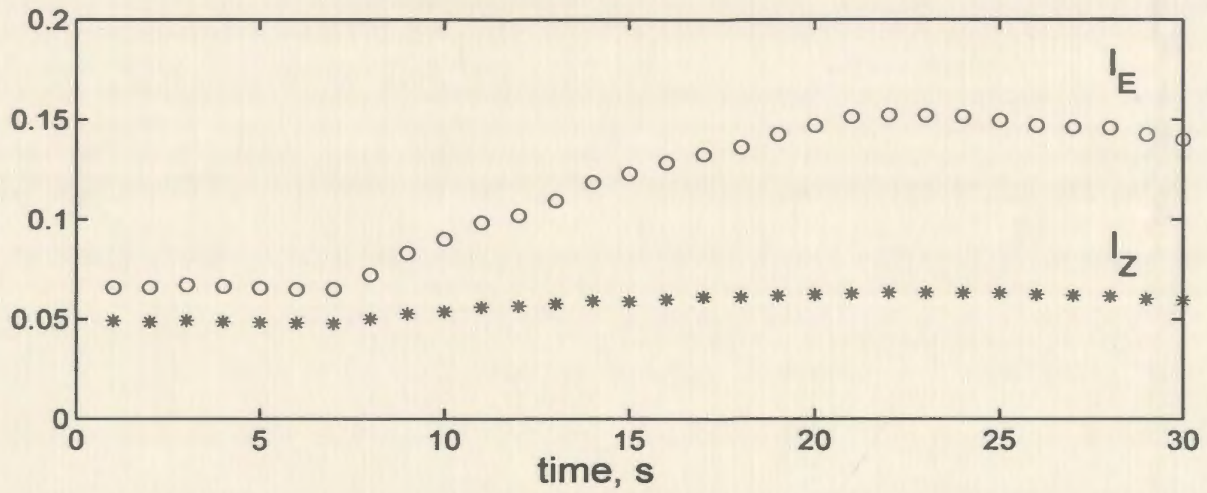


Figure 2.5: Energy-weighted mean scale l_E (circles) and enstrophy-weighted mean scale l_Z (stars) for experiments involving non-rotating turbulence.

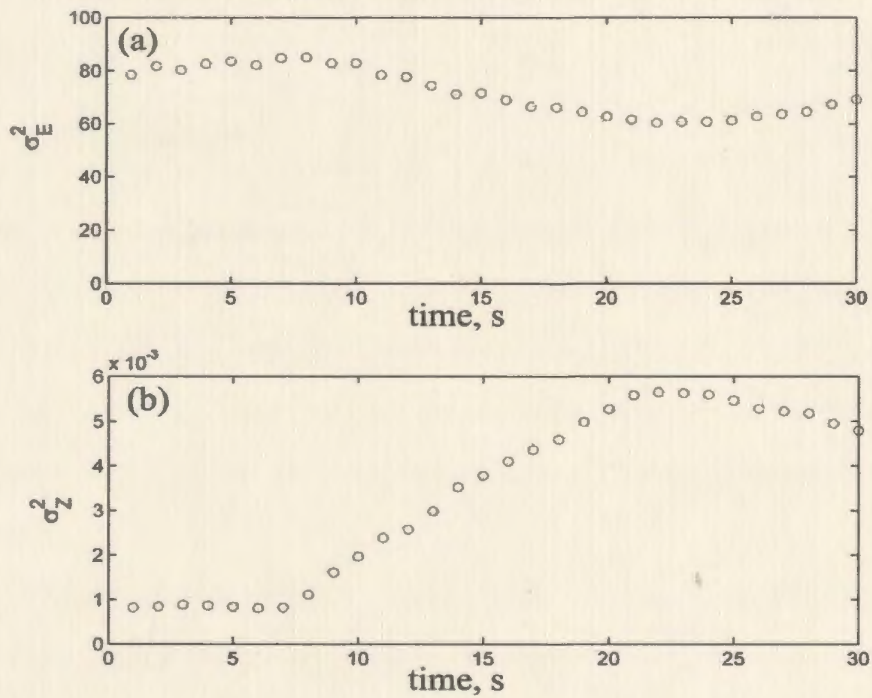


Figure 2.6: Variances of the spectrum σ_E^2 (a) and σ_Z^2 (b) for experiments involving non-rotating turbulence.

between the centers of the magnets in the array. Finally, once l_E reaches a value of $l_E = 0.15$, no further doubling occurs.

Figure 2.6 shows the temporal evolutions of the variances of the energy spectrum σ_E^2 and the enstrophy spectrum σ_Z^2 . From this figure we see that during the experiments σ_E^2 experiences no significant variation. Since the energy-weighted mean scale l_E grows, this indicates that the energy spectrum is shifting towards shorter wavenumbers while the width of the peak does not increase. Conversely, σ_Z^2 experiences linear growth at intermediate times of the flow evolution. Since the enstrophy-weighted mean scale l_Z remains approximately constant during the same period of time, this indicates that enstrophy is spreading in the wavenumber space while the “center of mass” of the distribution remains in place. This behavior is in agreement with the evolution of the enstrophy spectrum observed during intermediate times (figure 2.4).

2.4 Conclusions

In summary, it can be concluded that a laboratory investigation of decaying non-rotating two-dimensional turbulence has revealed the growth of the Reynolds number of the flow, which is in agreement with the predictions of Chasnov (1997). This growth provides additional evidence of the two-dimensional dynamics of the flow despite the fact that the thickness of the layer was somewhat higher than those used previously by other authors.

An investigation of the energy spectra of this flow demonstrated the upscale energy transfer via growth of subharmonic peaks due to successive pairing of vortex structures as well as through the growth of the energy-weighted means scale. This mechanism of growth of the vortex structures via successive pairing has been observed in other turbulent flows. Examples of such flows include turbulent flows in a thin layer of

fluid generated by an oscillating grid of thin vertical rods (Voropayev and Afanasyev, 1993, Voropayev et al., 1995) or the flow occurring due to gravitational instability in the form of an array of thermals propagating in a thin vertical cell (Voropayev et al., 1993).

For the high wavenumber part of the spectra, a power law decay of the form $E(k) \sim k^m$ was found. The value of this exponent is in agreement with classical theory. For the low wavenumber region of the spectra, the growth rate was found to be shallower than the scaling regime $m = 3$ which was predicted by Lesieur (1991) although the power law interval was not very pronounced in our experiments. The shallower decay rate is however in agreement with the results of experiments in soap films (Martin et al., 1998).

Chapter 3

Experimental Investigation of Beta-Plane Turbulence

3.1 Purpose

As was shown in previous chapters, one important characteristic and distinguishing feature of decaying two-dimensional turbulence that arises due to the conservation of energy is the presence of the inverse energy cascade. Through the energy cascade, energy that is injected into the initially turbulent system will flow from the small to the large length scales over the course of the consecutive merger of the constituent vortices. By studying two-dimensional turbulence on the beta-plane Rhines (1975) was able to extend the theory for two-dimensional turbulence to that of the large-scale geophysical turbulence found on a rotating sphere, such as the earth. On a rotating planet the effect of the Coriolis parameter will change according to the latitudinal position on the Earth's surface (beta-effect). Many large-scale structures that are present in the atmosphere and oceans can span several degrees of latitude and as such they are influenced by the changing Coriolis parameter. In his pioneering

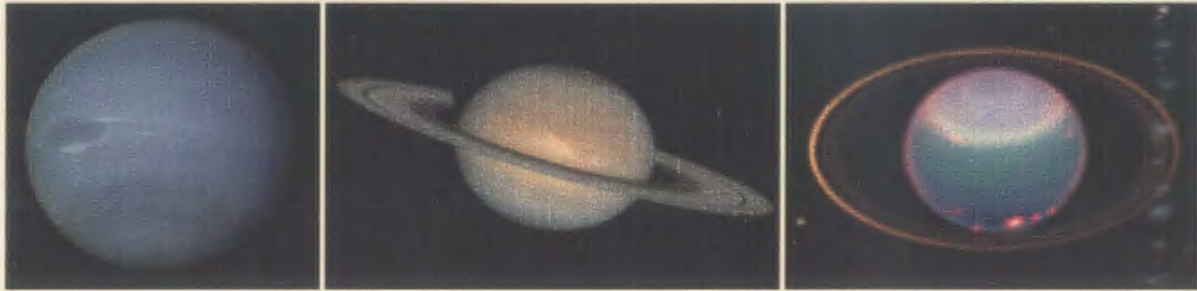


Figure 3.1: Zonal bands can be easily seen in photographs of the atmospheres of (a) Neptune. Image taken by Voyager 2 on its approach to Neptune (NASA/JPL-Caltech, 2004). (b) Saturn. This false color image of Saturn was taken by NASA's Hubble Space Telescope. In this infrared image, blue indicates a clear atmosphere, green indicates a thin haze and yellow a thicker haze above the main cloud layers. (Botha, 2004) (c) Uranus. A false-color image generated using data from the Hubble Space telescope's Near Infrared Camera and Multi-Object Spectrometer. In the image, the colors represent the height of the cloud layers where green and blue represents a clear atmosphere, yellow and grey represents a higher haze or cloud layer and orange and red indicates very high clouds. (Karkoschka, 2004)

study, Rhines found that when the quasi-two-dimensional turbulent flows occur on the beta-plane the inverse energy cascade is halted at some point by the formation of Rossby waves. The point at which the energy cascade is stopped corresponds to the Rhines scale (1975), which represents a boundary between the isotropic turbulent and anisotropic Rossby wave dominated regimes of the flow.

As a second effect of the varying Coriolis parameter with latitude on two-dimensional turbulence, Rhines predicted that the vortices that comprise the turbulence would experience a north-south redistribution leading to the formation of zonal jets and a transfer of energy to the zonal component. Zonal flows are prevalent in the Earth's atmosphere and oceans as well as in the atmospheres of other planets. The zonal bands that have been observed in the atmospheres of all the giant planets (Jupiter, Saturn, Neptune, and Uranus) provide obvious examples of these flows (figure 3.1). In fact, the Belts and Zones of Jupiter's atmosphere are quite frequently used to provide

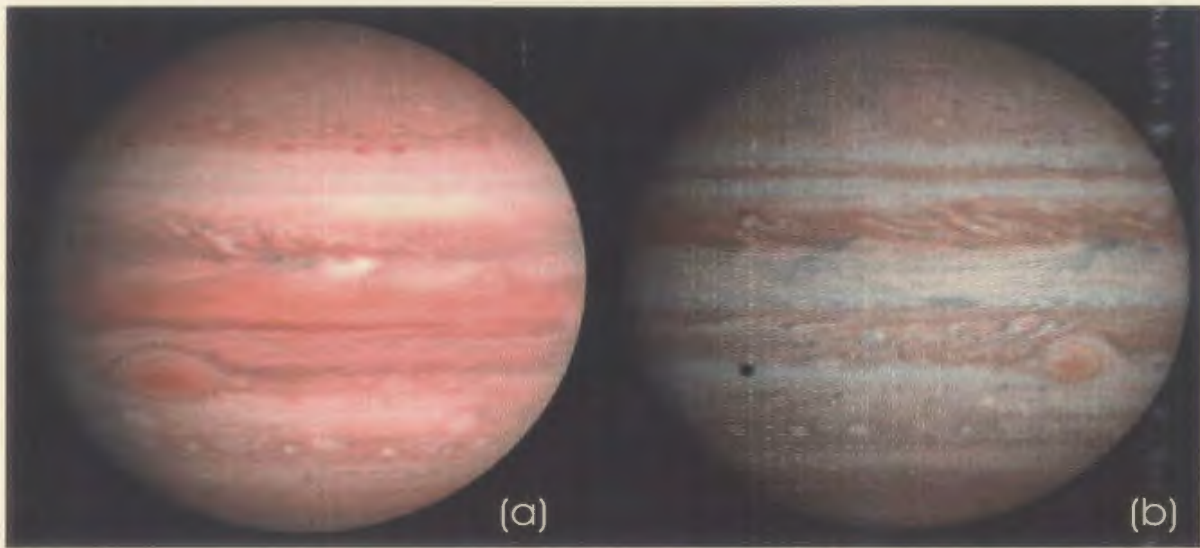


Figure 3.2: Zonation can be clearly seen in whole disk views of Jupiter. (a) The picture was taken by Voyager 2 in June 1979. (b) The image is from Cassini and was taken in November 2000. (Ingersoll et al., 2004)

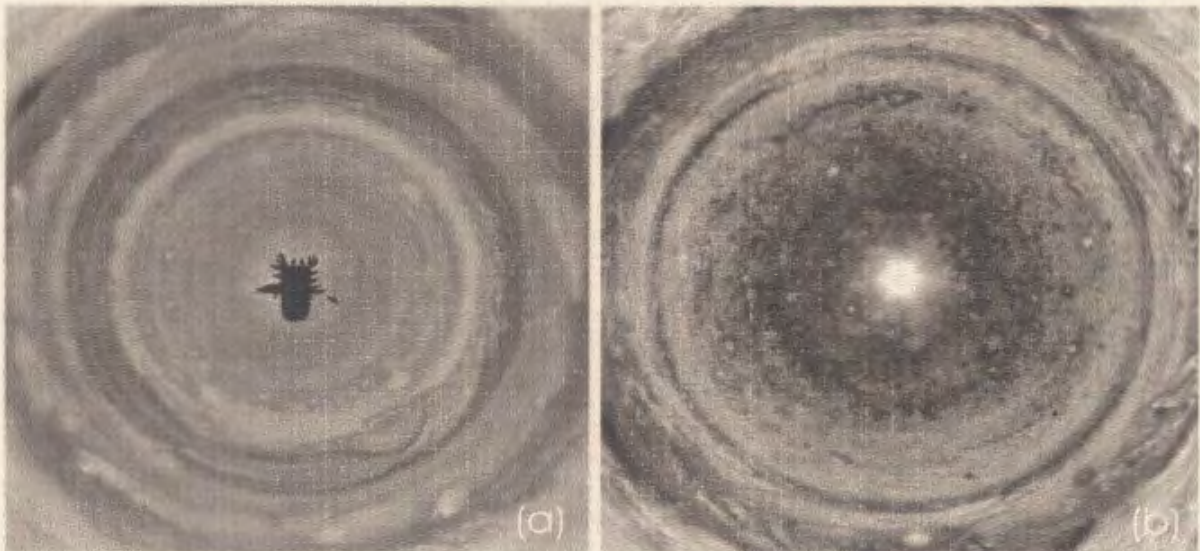


Figure 3.3: Two polar views of Jupiter in which images from different longitudes were map projected to show all the features in the polar region, in sunlight, at the same time. (a) South pole of Jupiter with images taken in 1979 from Voyager. (b) North pole of Jupiter with images taken in 2000 by Cassini. (Ingersoll et al., 2004)

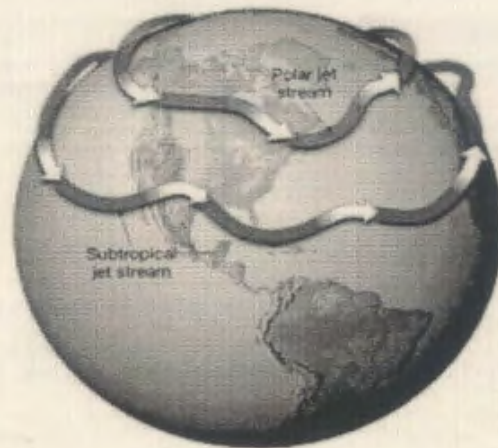


Figure 3.4: Schematic representation of the Jet streams that occur in the Earth's atmosphere and provide a local example of planetary zonal flows. (Poulsen, 2004)

an example in numerical studies on this subject due to the fact that it provides a much less complicated system than the Earth's atmosphere. Jupiter has a far greater number of eastward jet streams than does the Earth's atmosphere, since it has approximately six eastward jets in each hemisphere. Jupiter's atmosphere is comprised of white bands (zones) and dark bands (belts) with zonal jets that are strongest on the boundaries between these bands. Even though the belts and zones often vary in color and width, the number and magnitude of the jets have remained virtually unchanged, even through the presence of turbulence, convection and uncertainty in altitude. The zones and belts also contain many imbedded weather patterns (vortices) like the Great Red Spot and numerous other smaller vortices, which tend to have the same sense of rotation as the belt, or zone, in which they sit. These large scale-features tend to be steadier in time if they occur in the anticyclonic zones as opposed to the cyclonic belts (see figures 3.2 and 3.3). Jupiter also has a fluid interior, as opposed to a solid one, which means that these embedded vortices are not fixed

by topography and can last for centuries (Ingersoll et al., 2004).

The jet streams that occur in the Earth's atmosphere provide a more local example of the zonal jets (figure 3.4). In fact, both hemispheres on the Earth demonstrate two major jet streams, the polar jet stream and the subtropical jet stream. These jet streams typically flow from west to east and can in turn form separate branches. They have a typical length of thousands of kilometers and a width in the range of 160 to 500 km. These jet streams, strongly influence the Earth's climate and weather. In Canada, we are most affected by the polar jet stream whose position marks the location of the strongest temperature contrasts between polar and subtropical latitudes on the Earth's surface. The jet stream is not an evenly encircling latitude belt but rather is a flow that experiences significant undulations as masses of warm and cold air push away from their regions of origin. In this way, long wavelength waves called Rossby waves form in the jet stream that are obvious in weather maps as a series of three to six wave cycles (north-south undulations) in the jet stream. The positioning of the zonal and meridional components of the jet stream over the hemisphere strongly influences the temperature regimes experienced on the surface below. Under a zonal flow, the weather lies typically close to the climatological mean for that time of year. Typically, locations to the north of the jet stream will be relatively cold while locations to the south will be relatively warm. When under a meridional flow on the other hand, locations may experience temperatures that are unusual for that area. A trough (area of low pressure or cyclonic flow) in the Rossby wave tends to bring unusually cold temperatures to areas that are usually relatively warm and conversely, unusually warm temperatures develop in regions where it is normally relatively cold as a result of a crest (region of high pressure or anticyclonic flow) in the wave. Therefore, an understanding of the means by which Rossby waves develop in these zonal flows is of great importance.

Even though the dynamical process by which zonal flows form in the atmospheres of Earth and the giant planets remains poorly understood, it has been suggested (Read et al., 2004) that the zonation may arise out of anisotropy in a shallow turbulent layer of fluid due to the beta-effect. Until recently, most of the work that has been done in this area has consisted of numerical studies. Laboratory experiments however, provide an important means of studying these flows. As such, numerous aspects of the dynamics of beta-plane turbulence, especially the process of potential vorticity (PV) mixing, have recently been studied using experimental methods (Aubret et al., 2002). A detailed investigation of the spectral characteristics of the flow however has yet to be realized experimentally. The main difficulty involved in obtaining this goal has been the lack of sufficiently high resolution velocity fields of the flow. Therefore, the main purpose of the experiments on rotating turbulence presented herein is to demonstrate the occurrence of the dumbbell shaped two-dimensional spectra (lazy-8 in terminology by Holloway, 1984) by performing high resolution velocity measurements in a system with controlled forcing.

3.2 Experimental Set-Up and Procedure

The experiments which explore beta-plane turbulence were performed in a tank of inner dimensions $L = 34 \text{ cm}$ and $W = 31.5 \text{ cm}$ (figure 3.5) which contained a circular insert of inner diameter $2R = 31 \text{ cm}$. The container was filled with a single layer of salt water of height 1 cm and a concentration of 50 g/l. The flow was again forced electromagnetically, this time by imposing an electric current of magnitude 3A in the horizontal direction between two parallel electrodes located immediately outside of the circular insert. For this purpose, an array of 196 of the same magnets that were used in the previous experiments were arranged with equal spacing of 2 cm and

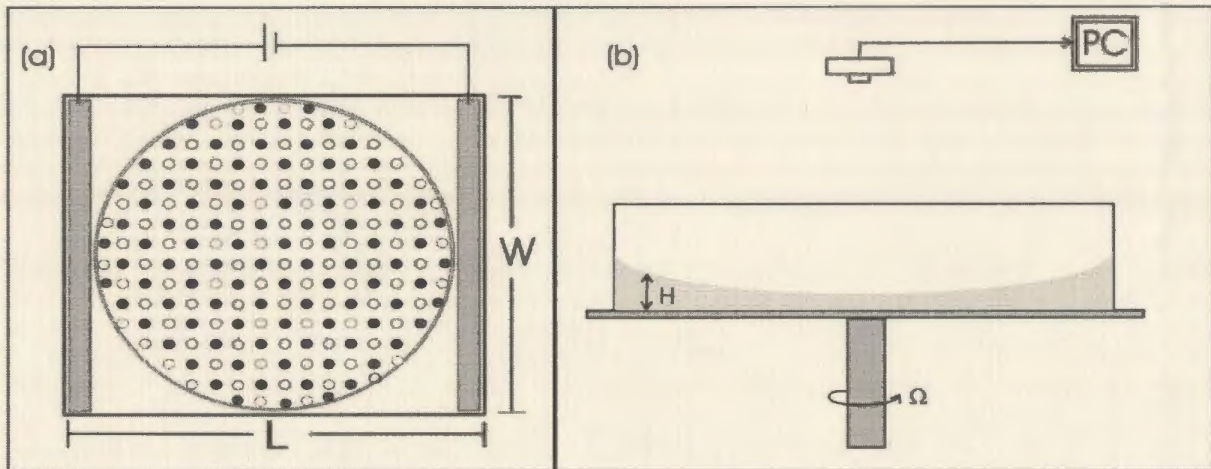


Figure 3.5: Sketch of the experimental setup used for the experiments involving rotating two-dimensional turbulence. (a) top view (b) side view.

alternating polarities immediately below a thin plastic sheet of thickness 0.02 cm that constituted the bottom of the container. In all of our experiments the flow was initially forced for a time period ranging between 5-10 minutes and then was allowed to decay freely after the current was switched off.

In order to simulate, in the laboratory, the effect of the varying Coriolis parameter felt by an ocean or atmosphere on a rotating sphere we used a standard method in which a rotating platform is used. Consider a shallow, homogeneous layer of fluid in a flat-bottomed annulus that is rotated at a constant angular speed Ω . Assuming that the center of the annulus corresponds to the center of rotation of the platform and that the fluid has a free surface it can be shown (Salmon, 1998) that away from the walls of the annulus and from any localized mass sources, the fluid is found to conserve its potential vorticity

$$\frac{D}{Dt} \left(\frac{f_0}{H} \right) = 0.$$

In this case however, the height $H = H(r)$ varies according to the radius r of the

annulus. This r -dependance is then analogous to the latitude dependance of $f = f(y)$ that is experienced by a system which has a constant H and a variable Coriolis parameter. In this way, the free-surface slope of the fluid in the rotating annulus imitates the beta-effect, with the center of the rotating table corresponding to the North-pole of a sphere. The experimental tank was rotated at rates that varied from stationary to 3.1 rads/s in an anti-clockwise direction around a vertical axis through its center. Once solid body rotation was achieved, the surface of the water achieved a parabolic shape such that the depth, H , of the layer was

$$H = H_0 + sr^2 \quad (3.1)$$

where $s = \Omega^2/2g$, Ω is the rotation rate of the platform, g is the gravitational constant, r is the radius and H_0 is the height of the fluid at $r = 0$. The value for H_0 was then calculated from the total volume of the fluid in the container and is given by

$$H_0 = z_0 - s \frac{(L^2 + W^2)}{12}, \quad (3.2)$$

where z_0 is the height of the fluid in the tank prior to rotation and L and W are the dimensions of the rectangular container. The experimental parameters for this set of experiments are summarized in Table 1. In most of the experiments (1-21 in Table 1) z_0 was chosen to be 1 cm. In experiments 22-26 (Table 1) the lower value of $z_0 = 0.7$ cm was used. The same value of the fluid layer depth was used in our previous experiments with non-rotating two-dimensional turbulence (Wells and Afanasyev, 2004) and was shown to be large enough for the system not to be too dissipative. In experiments 22-26 (Table 1) the lower value of $z_0 = 0.7$ cm was used to obtain higher dissipation rate for comparison.

Experiment Number	$\Omega(s^{-1})$	$S = \Omega^2/2g$ (cm^{-1})	$H_0(cm)$	$D(cm)$	$\beta(cm^{-1})$	$2\lambda(s^{-1})$
1	3.1	0.0049	0.18	0.57	0.97	0.36
2	3.1	0.0049	0.18	0.57	0.97	0.33
3	3.1	0.0049	0.18	0.57	0.97	0.36
4	2.8	0.0041	0.32	0.64	0.63	0.32
5	2.8	0.0041	0.32	0.64	0.63	0.35
6	2.6	0.0034	0.44	0.70	0.41	0.30
7	2.6	0.0034	0.44	0.70	0.41	0.31
8	2.5	0.0033	0.45	0.71	0.40	0.39
9	2.3	0.0027	0.55	0.76	0.27	0.28
10	2.3	0.0027	0.55	0.76	0.27	0.27
11	2.0	0.0021	0.64	0.81	0.17	0.27
12	2.0	0.0021	0.64	0.81	0.17	0.29
13	1.8	0.0016	0.73	0.86	0.11	0.24
14	1.8	0.0016	0.73	0.86	0.11	0.25
15	1.5	0.0012	0.80	0.90	0.063	0.22
16	1.5	0.0012	0.80	0.90	0.063	0.22
17	1.3	8.1×10^{-4}	0.86	0.93	0.034	0.19
18	1.3	8.1×10^{-4}	0.86	0.93	0.034	0.20
19	1.0	5.1×10^{-4}	0.92	0.96	0.016	0.18
20	0.47	1.1×10^{-4}	0.98	0.99	0.0017	0.14
21	0.0	0.0	1.0	1.0	0.0	0.074
22	2.6	0.0034	0.14	0.40	0.78	0.50
23	2.0	0.0021	0.34	0.51	0.28	0.46
24	1.8	0.0016	0.43	0.56	0.17	0.44
25	1.5	0.0012	0.50	0.60	0.095	0.33
26	1.0	5.1×10^{-4}	0.62	0.66	0.024	0.30

Table 3.1: Experimental parameters for experiments on rotating turbulence.

Instantaneous horizontal velocity fields of the flow were again measured using Particle Imaging Velocimetry (PIV). The tracer particles used in these experiments were small spheres of dyed wax with an average diameter of 1 mm and a density slighter less than that of the salt water. The density of these beads was such that when added to the tank, they floated on top of the water and followed the flow. To produce a high contrast between the beads and the plastic bottom, the container was lit from above with two lamps. Videos of this set of experiments were recorded in plan view using a digital video camera with an array resolution of 1032 x 1032 pixels. The typical spatial resolution of the images was 35.5 pixels/cm. The camera was fixed to the rotating platform to obtain images in the same frame of reference as the experimental tank and the videos were recorded directly into the memory buffers of a computer also situated on the rotating platform. Further processing of images was performed on workstations with dual Alpha processors where successive images with a frame rate of 8.5 fps were used to obtain 4.25 velocity fields per second.

3.3 Results and Discussion

In the case of our second set of experiments involving beta-plane turbulence, the typical decay rate of the total energy was measured during an intermediate time of 5 s after forcing ceased. Recall that bottom friction is commonly parameterized by a linear term in the vorticity equation

$$\frac{D\omega}{Dt} = -\lambda\omega + \nu\nabla^2\omega,$$

where ω is the vorticity, λ is the linear drag coefficient and ν is the kinematic viscosity. For a rotating system, λ can be expressed as $\lambda = fE^{1/2}/2$. Equivalently, the

characteristic Ekman time scale is $T_E = \lambda^{-1} = H/(\nu\Omega)^{1/2}$. The Ekman condition is valid for flows with low Rossby number. It works well however even for vortices with moderate Rossby number (e.g. Kloosterziel and van Heijst, 1992, Maas, 1993). Linear drag causes an exponential decay of energy. The contribution of the ordinary viscosity to the decay rate for these experiments remains approximately the same as it had been in the non-rotating case. The typical decay rate of the total energy however is much greater in the rotating case and so in this case bottom friction prevails. This faster decay rate arises because in the experiments involving beta-plane turbulence we use a single layer of fluid instead of the two-layer system that was used to shield the flow from the bottom of the container in experiments with non-rotating turbulence. Also, the linear drag coefficient is linearly proportional to the rotation rate Ω of the system since the average depth of the layer, given in our case by

$$D = \frac{1}{R} \int_0^R H(r) dr = H_0 + \frac{sR^2}{3}$$

decreases with rotation rate (see Table 1).

Thus for the case of the rotating turbulence we have

$$2\lambda \approx \frac{d(\ln E)}{dt}.$$

The values of the linear drag coefficient 2λ for the experiments performed with beta-plane turbulence are given in table 3.1.

First, the general features of the flow for the case of β -plane turbulence were analyzed. The sequence of plots shown in figure 3.6 shows the typical flow evolution for an experiment with a high value of β in terms of the vorticity (color) and velocity (arrows) at various times. During forcing, the flow is characterized by isotropic

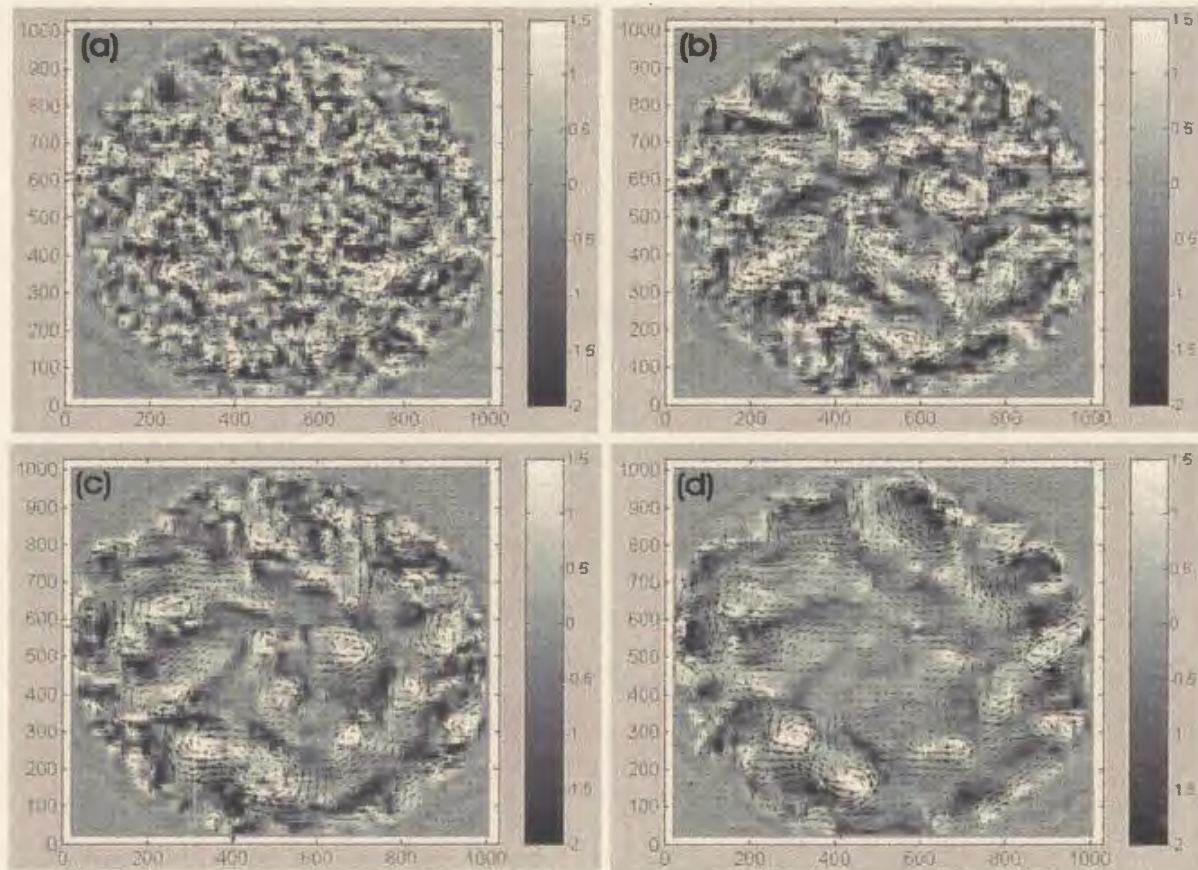


Figure 3.6: Sequence of plots that show the typical flow evolution for an experiment with a high value of β ($\Omega = 3.15 \text{ s}^{-1}$) in terms of the vorticity (color) and velocity (arrows) at various times. (a) $t = 0.5 \text{ s}$ (b) $t = 1.5 \text{ s}$ (c) $t = 3 \text{ s}$ (d) $t = 4 \text{ s}$

turbulence with vortices of both rotational senses distributed evenly throughout the container. Once the forcing is stopped however, the vortices begin to merge/pair with neighbors of like rotational sense. Finally, the vortices begin to rearrange themselves into an anisotropic flow such that a series of bands of vortices form zonally that alternate between vortices with positive and negative rotational sense. The placement of these bands of vortices is such that zonal jets are formed between the bands. This behavior is in agreement with the predictions of Rhines (1975) who predicted the anisotropization of the flow field and a stabilization of the zonal flow due to the beta-effect. This behavior is markedly different than that of non-rotating two-dimensional turbulence due to the fact that the beta-plane acts as a potential vorticity selector (Aubert et al., 2002) because of the conservation of potential vorticity (equation 1.18). As the flow evolves, cyclones (vortices that rotate in the same sense as the system) cannot move outwards because this motion triggers the formation of a Rossby wave that forces them back into their original position. On the other hand, nothing prevents the cyclones from moving towards the center of the container. In the same way, anticyclones (vortices that rotate in the opposite sense as the system) are prevented from moving towards the center of the container but not from moving outwards (figure 3.6). It is interesting to note that in the final stages in the flow evolution of these experiments, pictures of the flow bear notable similarities to weather maps at the 500-millibar level which show the positions of the jet streams as well as high and low pressure systems (e.g., figures 3.7 and 3.8).

The evolution can then be further examined through a *Hovmoller plot* which demonstrates the evolution of the zonally average flow as a function of both time and radius is given by figure 3.9 for an experiment with a high value of β . This plot reveals that after an initial period of forcing, the vortices in the turbulent flow redistribute

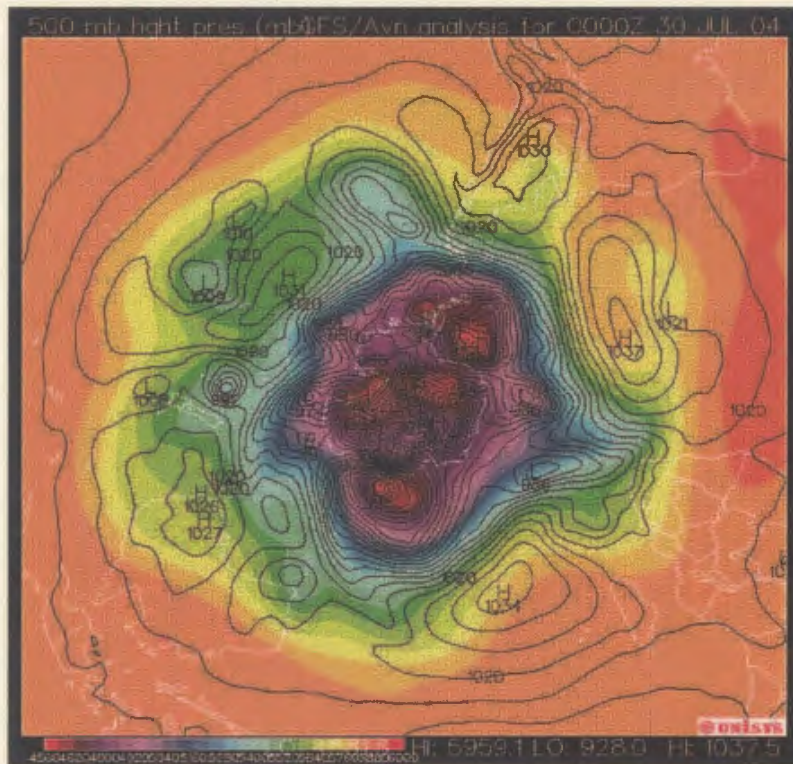


Figure 3.7: 500 millibar weather map of the Southern Hemisphere which shows the positions of the jet streams as well as high and low pressure systems. The figure represents a composite 500 mb height (color) and sea level pressure map of data taken on July 30, 2004 by Unisys Corporation (Unisys Weather, 2004).

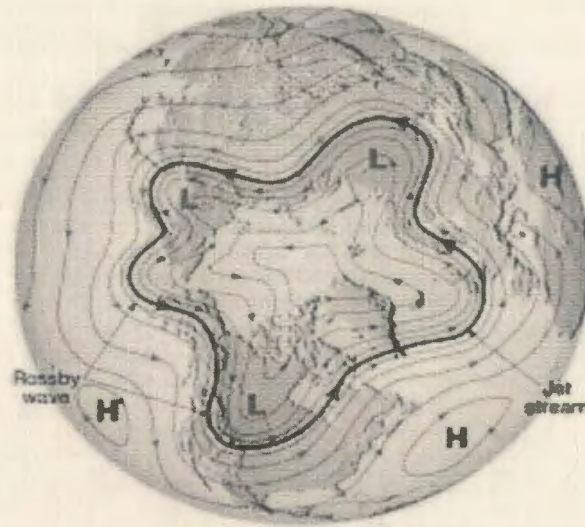


Figure 3.8: Schematic 500 millibar weather map of North America that shows the positions of the jet streams as well as high and low pressure systems. (Poulsen, 2004)

themselves such that two prograde (cyclonic) and two retrograde (anti-cyclonic) jets develop. Eventually, these jets merge into a system that consists of a weak retrograde circulation in the center of the domain surrounded at its periphery by a relatively strong prograde jet.

Typical potential vorticity (color) and velocity (arrows) fields are then given in figure 3.10 for two experiments with high and low values of β . The pictures represent an intermediate time in the flow evolution shortly after the forcing was stopped. As predicted, the pictures show clear difference between the two flows. For the experiment with the low value of β (figure 3.10 b), the potential vorticity is mixed to a significant degree and the flow closely resembles non-rotating isotropic turbulence. On the other hand, the experiment with the high value of β (figure 3.10 a) clearly shows the anisotropic behavior typical of β -plane turbulence. This flow is charac-

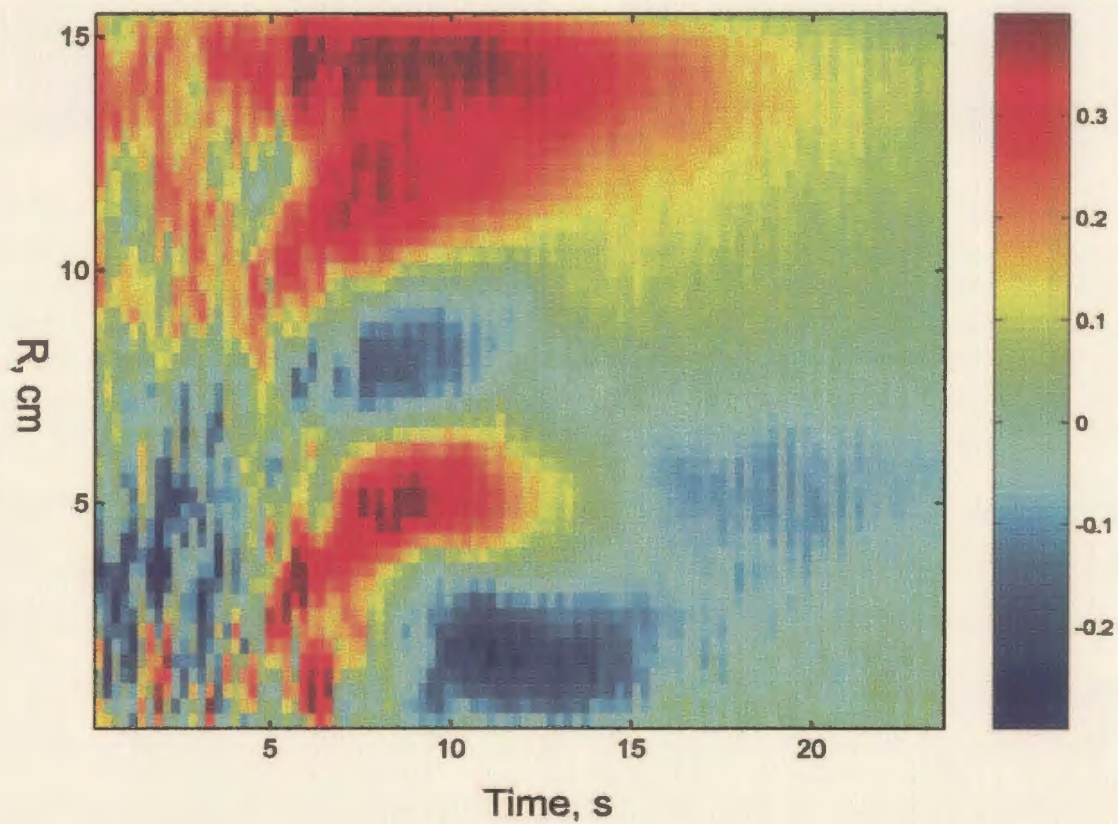


Figure 3.9: Space-time diagram of the averaged zonal velocity for experiment 15 (Table 3.1). Scale represents velocity in cm/s.

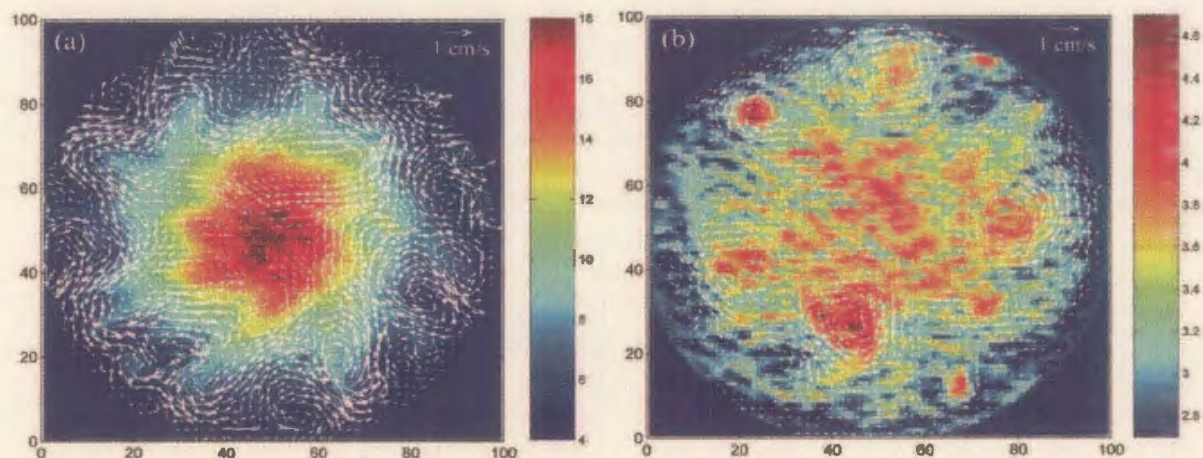


Figure 3.10: Vorticity (color) and velocity (arrows) fields measured in two experiments with high and low beta: experiment 5 (Table 3.1) at $t = 4$ s after the forcing was stopped (a) and experiment 15 at $t = 11$ s (b). The color bar shows the potential vorticity scale in $(\text{cm/s})^{-1}$. The arrow in the top left hand corner of each frame represents the velocity scale, 1 cm/s . The total distance in x and y axes is 31 cm .

terized by a well-defined polar vortex that resembles the one found in the Earth's atmosphere where it develops as a strong area of low-pressure above the core of the coldest polar air (figure 3.8). The experimental polar vortex has an intense prograde jet at its periphery that is subject to wave-like perturbations of significant amplitude that represent a typical Rossby wave. The perturbations can be considered as a vortex Rossby wave (Montgomery and Kallenbach, 1997, Montgomery and Lu, 1997) since it develops with significant background shear. An animated sequence of images of this flow shows that the wave is almost stationary so that its phase moves only very slowly in the cyclonic direction. It is also clear that the vortices that constitute protuberances at the periphery of the polar vortex in figure 3.10 a are elongated. This is in accordance with the predictions made by Rhines (1975) who predicted that one of the effects of planetary rotation on two-dimensional turbulence would be a preference for the vortices in the flow to become zonally elongated. This is in contrast to the

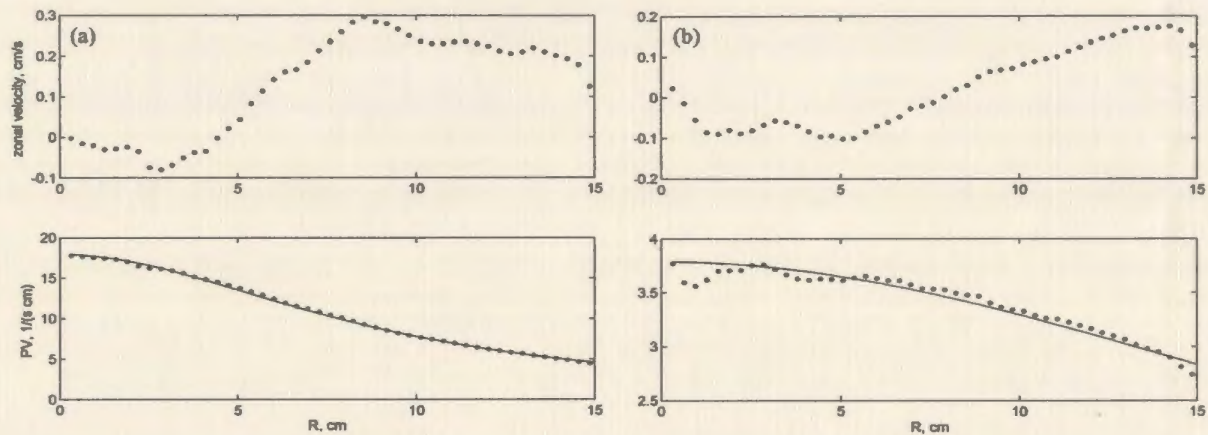


Figure 3.11: Radial distributions of azimuthally averaged zonal velocity and potential vorticity for two experiments with high and low beta: experiment 5 (Table 3.1) at $t = 4s$ after the forcing was stopped (a) and experiment 15 at $t = 11s$ (b). Solid lines represent distributions of planetary vorticity f/H .

vortices in the flow in figure 3.10 b which are round owing to the fact that for low value of β , the flow is not significantly effected by rotation.

Plots of the radial distributions of azimuthally averaged zonal velocity and potential vorticity for the two experiments are given in figure 3.11. The plot of the distribution of the zonally averaged azimuthal velocity for the experiment with the high value of β confirms this behavior. The plot shows a narrow prograde jet localized near $r = 8$ cm and a weak retrograde circulation in the center of the container that represents the polar vortex. The corresponding plot of zonally averaged potential vorticity (figure 3.11) demonstrates that the potential vorticity in the flow with higher β is not mixed to any noticeable extent since the values of potential vorticity are consistent with the solid line which represents the distributions of planetary vorticity f/H . The perturbations of the polar vortex are therefore “elastic” in accordance to theoretical results. The plot of zonally averaged potential vorticity (figure 3.11) for

the flow with low β on the other hand, demonstrates several plateaus where the values of zonally averaged potential vorticity do not lie along the line of f/H . These regions represent the mixing of the potential vorticity that is expected for non-rotating turbulence but is not consistent with classical theory for β -plane turbulence. It is also evident that the mixing is stronger in the center of the container where the gradient of the background vorticity f/H is weaker than that at larger radii.

The flows with high and moderate values β demonstrated another interesting phenomenon of geophysical relevance, namely the "blocking" of the jet. Atmospheric blocking is a persistent weather phenomenon that arises as an interruption of the normal west-to-east flow at mid to high latitudes. This blocking occurs approximately one to three times each Northern Hemisphere winter (and occasionally during other seasons) when large high-pressure anticyclones form and usually persist for at least 10 days and sometimes longer than a month (O'Connor, 1963, Dole and Gordon, 1983, Cheng and Wallace, 1993). The effect of these anticyclones then is to block the nearly zonal flow and deflect it towards the north pole. It has also been found that certain atmospheric anomalies, such as persistent blocking events are for the most part barotropic or nearly two-dimensional (Cheng and Wallace, 1993, Charney and Devore, 1979, Lau and Nath, 1987). The type of blocking anomaly visible in our experiments represents the so-called "Omega" block, which is a high-pressure anticyclone that has become displaced and is on the poleward side of the jet stream. This type of blocking gains its name due to the fact that when analyzed on upper air charts its shape resembles that of the Greek letter Ω . An example of this type of blocking event is shown in figure 3.12 for atmospheric flow in the Northern Hemisphere. The figure shows the contrast between an almost zonal flow and that of a blocked flow. In the case shown in this figure the effect of the blocking pattern is to advect cold Arctic air southward over eastern North America or Europe while decreasing precipitation

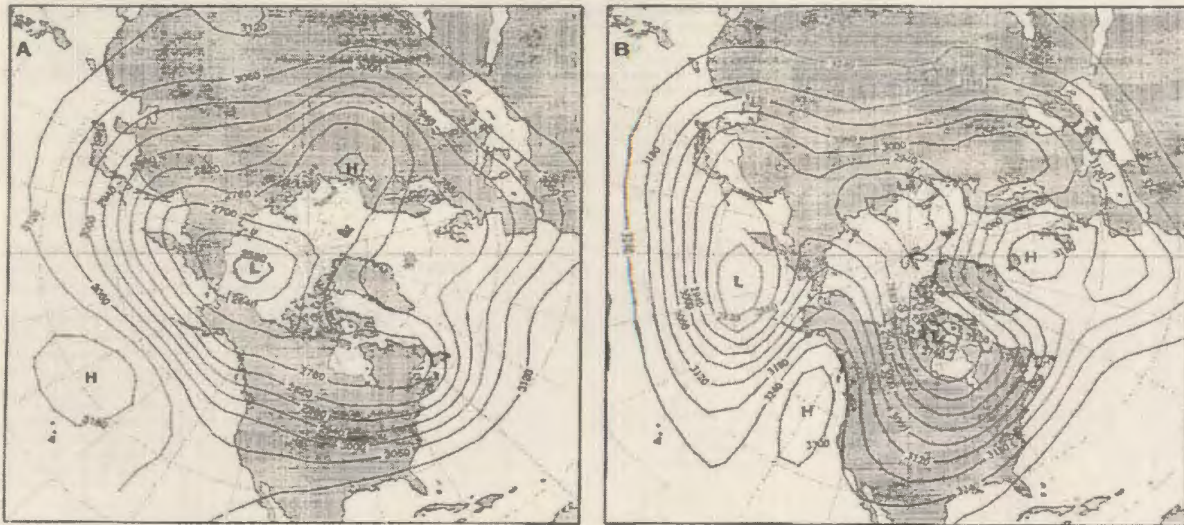


Figure 3.12: 700 millibar weather map of North America. (a) Unblocked flow (b) Blocked Flow. The plots represent an averaging over 10 days of twice-daily data from the National Oceanic and Atmospheric Administration's Climate Analysis Center. (a) represents data taken from December 13 to 22, 1978. (b) represents data taken from January 10 to 19, 1963 and shows how the blocked flow sends cold air southward over eastern North America or Europe and decreases precipitation in the continent's western part. (Weeks et al., 1997)

in the continent's western part (Weeks et al., 1997).

One of the most obvious examples that occurred in our experiments is shown in the vorticity plot in figure 3.13. This blocking event occurred as a result of the entrainment of a patch of lower potential vorticity between two protuberances. A vortex dipole with a direction opposite to that of the jet was formed and then remained stationary in the jet splitting it into two branches. Our experimental blocking event lasted for approximately two rotations of the system (or two laboratory days), which is a relatively short period of blocking when compared to blocking events in the Earth's atmosphere that can last as long as a few weeks. The relatively short time period of

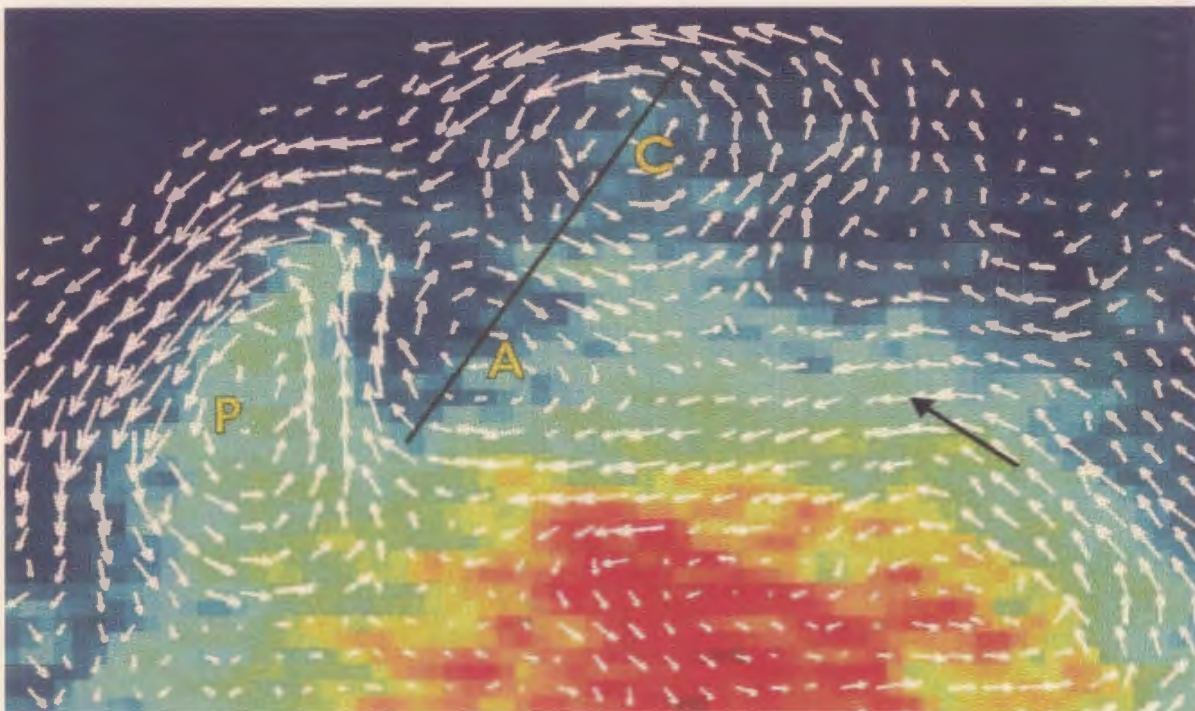


Figure 3.13: Zoomed velocity and potential vorticity map for experiment 10 (Table 3.1) demonstrating a laboratory blocking event, $t = 8s$ after the forcing was stopped. The significant features of the flow are highlighted. The anticyclonic (A) and cyclonic (C) vortices that comprise the stationary dipole are marked as is a protuberance (P) at the periphery of the polar vortex. The solid line represents the line through the center of the dipole along which the distribution of PV was measured and the black arrow represents the direction of the zonal flow.

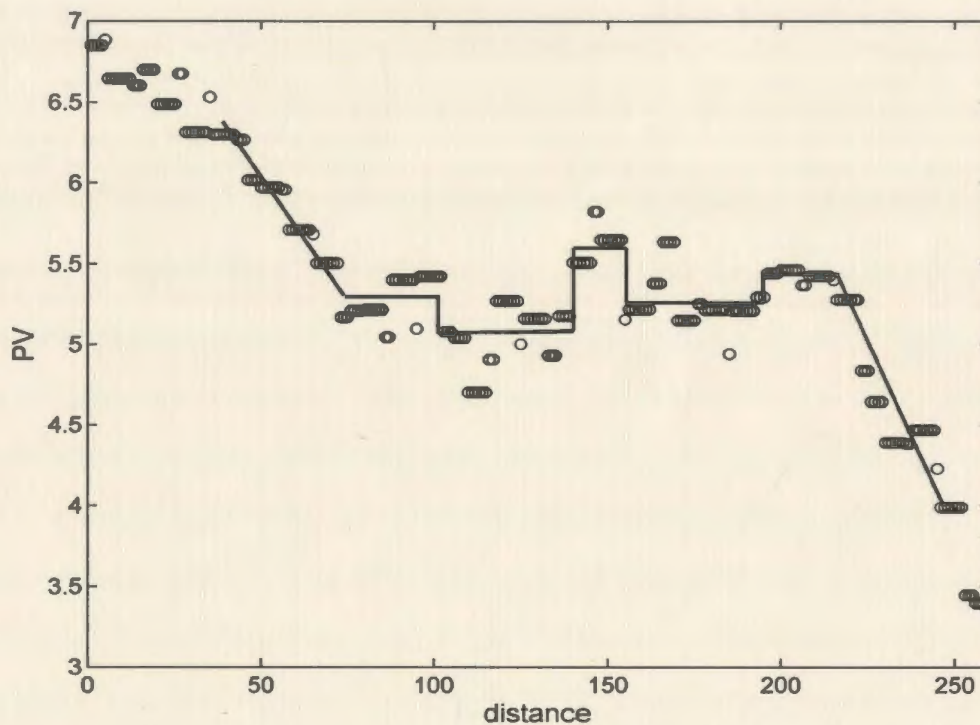


Figure 3.14: Distribution of potential vorticity along the straight line going through the centers of vortices in the dipole in Fig. 3.13. The distribution is approximated by a piecewise linear dependence (solid line).

our blocking event however is most likely due to the fact that the flow itself is not stationary in our case.

An analysis of the distribution of the potential vorticity along a line that crosses the centers of the constituent vortices of the dipole that forms with a direction opposite to that of the jet was performed (figure 3.14). The analysis revealed a few interesting features of this structure. The figure shows that outside of the dipole there is a strong gradient of potential vorticity and that the jets surrounding the dipole are characterized by a uniform distribution of potential vorticity. The protrusions in between the vortices of the dipole on the other hand contain a relatively

high potential vorticity. It is also obvious that as is expected, the left hand (anticyclonic) vortex of the dipole contains a relatively lower potential vorticity than that of the right hand (cyclonic) vortex.

Finally, we performed an analysis of the spectral characteristics of the experiments on beta plane turbulence. For these experiments, the velocity components (v_x, v_y) were measured on the same regular Cartesian grid of dimensions 99×99 that was used for the experiments on non-rotating turbulence. In this series of experiments however the turbulent flows were generated in an annulus as opposed to in a square container and so it is more natural to use a cylindrical polar coordinate system (r, θ) for the spectral analysis. To this end, the measured velocity field was linearly interpolated onto a polar grid of dimensions 48×96 . The spacing between the grid points in the radial direction in the new polar grid was approximately consistent with those in the Cartesian grid. On the other hand in the azimuthal direction the data was undersampled at larger radii and oversampled near the center of the domain. Finally, the radial and azimuthal components of the velocity field (v_r, v_θ) were estimated on the polar grid.

For each component of the velocity (v_r, v_θ) , the two-dimensional power spectra $E_{mn} = v_{mn}v_{mn}^*$ in wavenumber space (m, n) were then calculated. Here, time averaging was performed at intervals of 1 s. Each velocity component (v_r, v_θ) was decomposed using a Fourier transform in θ and Bessel function decomposition in r to give

$$v(r, \theta) = \sum_m \sum_n v_{mn} e^{im\theta} J_n \left(\alpha_{mn} \frac{r}{R} \right).$$

Here, the Bessel coefficients were obtained numerically by using the formula (Arfken, 2001)

$$v_{mn} = \frac{2}{R^2 [J_{n+1}(\alpha_{mn})]^2} \int_0^R v_m(r) J_n \left(\alpha_{mn} \frac{r}{R} \right) r dr.$$

For this analysis, we have introduced the one-dimensional wavenumber $k = \alpha_{mn}/R$ which is analogous to the radial wavenumber $k = (k_x^2 + k_y^2)^{1/2}$ that is defined for the two-dimensional Fourier transform in Cartesian coordinates. This wavenumber may be obtained from the comparison of the result of the application of the Laplacian operator on the basis functions $\phi_{mn} = e^{im\theta} J_m\left(\alpha_{mn} \frac{r}{R}\right)$ such that $\nabla^2 \phi_{mn} = -\alpha_{mn}^2 \phi_{mn}$, with the corresponding equation for the two-dimensional Fourier series (Boer, 1983).

The series of 26 experiments that were performed involving beta-plane turbulence cover a range of rotation rates and consequently a range of values of β . As such, it is of interest to examine the evolution of these flows at high and low values of β . The two-dimensional energy spectra E_{mn} for two experiments with different values of β , are given in figure 3.15. It is easy to see from this figure that for the experiment with a low value of β (figure 3.15 b), the spectrum is aligned along the isolines of the one-dimensional wavenumber k given by the solid white lines. This behavior indicates that in this case the flow is approximately isotropic. For the experiment with the higher value of β however, the spectrum does not align with the isolines of k . This behavior is consistent with the anisotropic spectrum that is predicted at high values of β due to the presence of Rossby waves.

Recall that the dispersion relation for Rossby waves is anisotropic and can, in our case, be defined as

$$\omega = \frac{\beta m}{r_0 k^2}$$

where ω is the wave frequency and $r_0 = R/2$ is an intermediate radius which has been introduced in order to estimate the dimensional azimuthal wavenumber m/r_0 . For our estimates, we reintroduce the turbulent frequency as $\sigma = kV_{rms}$, where the root mean square velocity is given by $V_{rms} = (2E)^{1/2}$. If we then take the ratio of the

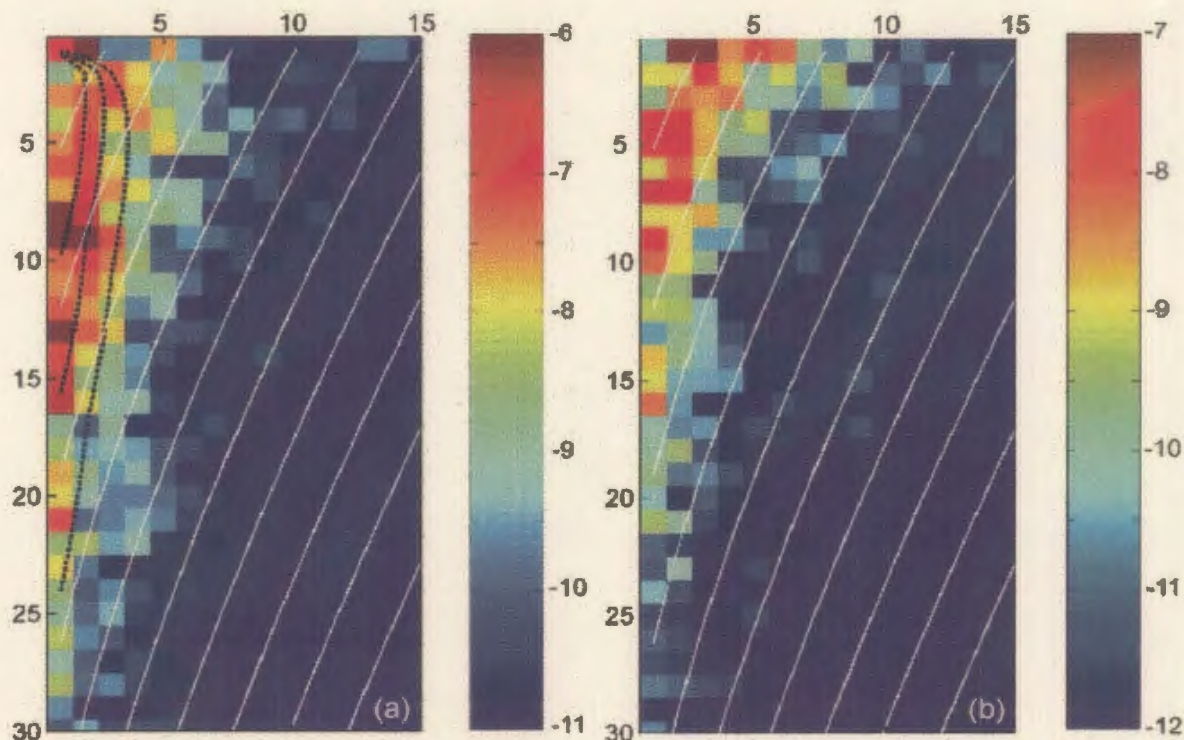


Figure 3.15: Two-dimensional energy spectra for two experiments with high and low beta: experiment 1 (Table 3.1) at $t = 4s$ after the forcing was stopped (a) and experiment 15 at $t = 11s$ (b). Color scale represents $\ln(E_{mn})$. The vertical axis represents index m such that the first (top) line of the diagram shows the zonal spectrum. Solid white lines are isolines (from 0.5 to 5 with the interval 0.5 cm^{-1}) of the one-dimensional wavenumber $k = \alpha_{mn}/R$. Dashed white lines represent anisotropic wave-turbulence boundary in wave vector space given by equation (3.3). Contours corresponding to values of 0.5, 1 and 2 are shown.

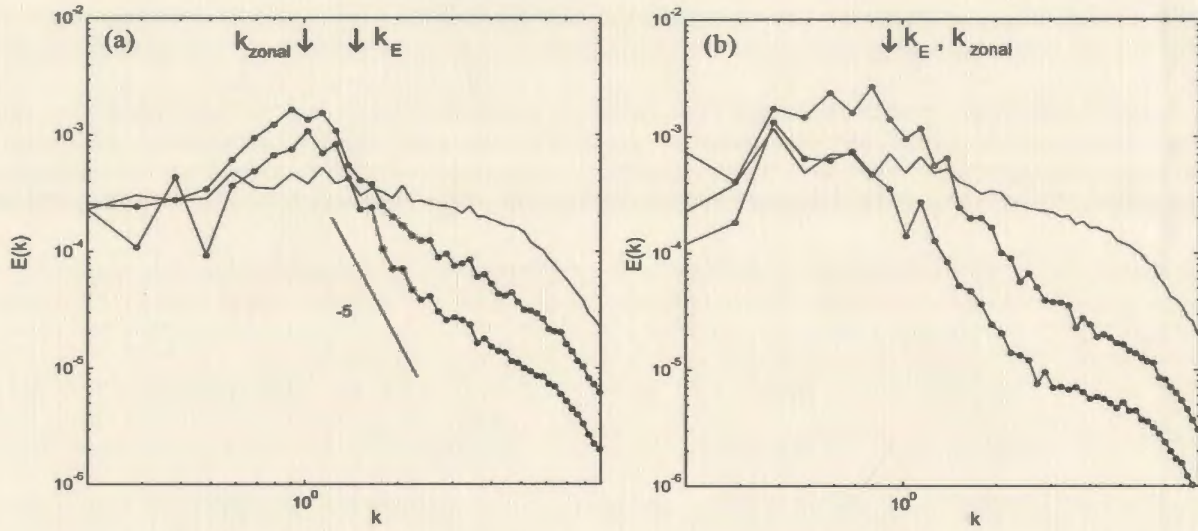


Figure 3.16: Evolution of the one-dimensional energy spectrum for two experiments with high and low beta: experiment 1 (Table 3.1) (a) and experiment 15 (b). Solid lines represent the spectra during the forcing. Grey and black circles show spectra at $t = 2, 4s$ after the forcing was stopped (a) and $t = 1.5, 7s$ (b). Arrows indicate the position of the centroid of the total energy and zonal energy distributions.

wave frequency and the turbulent frequency we obtain

$$\frac{\omega}{\sigma} = \frac{2\beta m}{Rk^3 V_{rms}}. \quad (3.3)$$

Assuming that this ratio is of the order of unity we obtain the anisotropic *Rhines barrier* (Rhines, 1975) between the wave and the turbulence dominated regions of the spectrum. The dependence of equation (3.3) in (m, n) space for three values of the ratio ω/σ is shown as the dotted line in figure 3.15. These isolines represent the analogue of the dumbbell shaped (lazy-8) two-dimensional spectrum in polar coordinates. It is predicted that Rossby waves are dominant within these curves and it is shown in figure 3.15(a) that the spectrum is consistent with the isolines of ω/σ .

The one-dimensional total energy spectrum $E(k)$ is then obtained by sorting the

elements of the array E_{mn} according to the value of the corresponding wavenumber $k = \alpha_{mn}/R$. The zonal energy $E_Z(k)$ is represented by the first line ($m = 0$) of the array E_{mn} . The typical evolution of this one-dimensional energy spectrum was then plotted for two experiments with different rotation rates and consequently different values of β (figure 3.16). The solid lines in this figure represent the spectra during the forcing period and it is clear that the spectra during forcing are very similar for both experiments. It is also obvious that the energy is distributed evenly over the entire range of the wavenumbers for the experiments. The circles in this figure represent the spectra for the decaying flows and this is the part of the spectrum that we will now study. The most obvious difference in this part of the spectrum between the two experiments is the position of the spectral peaks. As predicted, the position of the spectral peak is at a higher wavenumber for the experiment with the higher value of β than it is for the experiment with the low value of β . Another interesting difference between the spectra is that the spectral peak for the experiments with low β shifts towards lower wavenumbers with time whereas the peak for the experiment with higher β remains in the same position. The shift in the spectral peak observed for the experiments with low β is constant with the experiments performed using non-rotating turbulence. As was the case with the non-rotating turbulence, the shift corresponds to pairing of the original vortex structures in the flow such that the subharmonic peak grows while the original peak diminishes. The lack of a shift in the spectral peak for the experiment with higher β is consistent with the fact that the presence of the β -effect tends to restrict vortex pairing in favor of the creation of zonal motions. Finally, the shape of the energy spectrum for the experiment with higher β has the form $E(k) \sim k^m$, where $m \cong -5$ for the high wavenumber part of the spectra. This value is in agreement with theory (equation 1.29). In the experiment with the lower values of β , a slower decay of the energy spectrum is observed. The high wavenumber

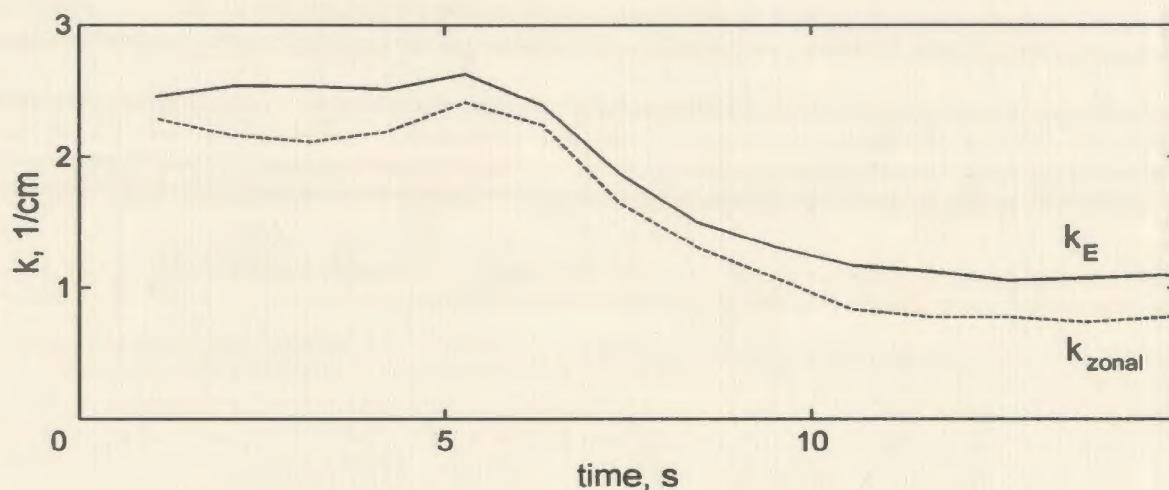


Figure 3.17: Evolution of energy-weighted mean scale k for total energy (solid line) and for zonal energy (dashed line) in the experiment 7 (Table 3.1).

part of this spectra is consistent with the power law of the form k^{-3} which is similar to that observed in experiments with nonrotating two-dimensional turbulence. As one might expect the small scale vortices are unaffected by the system rotation. This is consistent with the fact that for low values of β , the flow should behave more like non-rotating two-dimensional turbulence for which a slower spectrum decay rate is predicted. The result is also consistent with the shifting of the spectral peak that was observed for this experiment.

As with the non-rotating turbulence, we will now examine the energy-weighted mean wave number k_E which is defined previously in equation (2.3) as well as the similar wavenumber k_{Zonal} which is defined in the same way for the zonal energy spectrum. Here again we estimate these integral characteristics through numerical integration of the appropriate moments of the one-dimensional energy spectra (equation 2.2). Figure 3.17 shows the typical time evolutions of k_E and k_{Zonal} for experiment 7 in table 3.1. Both of the wavenumbers remain at a constant value during forcing and

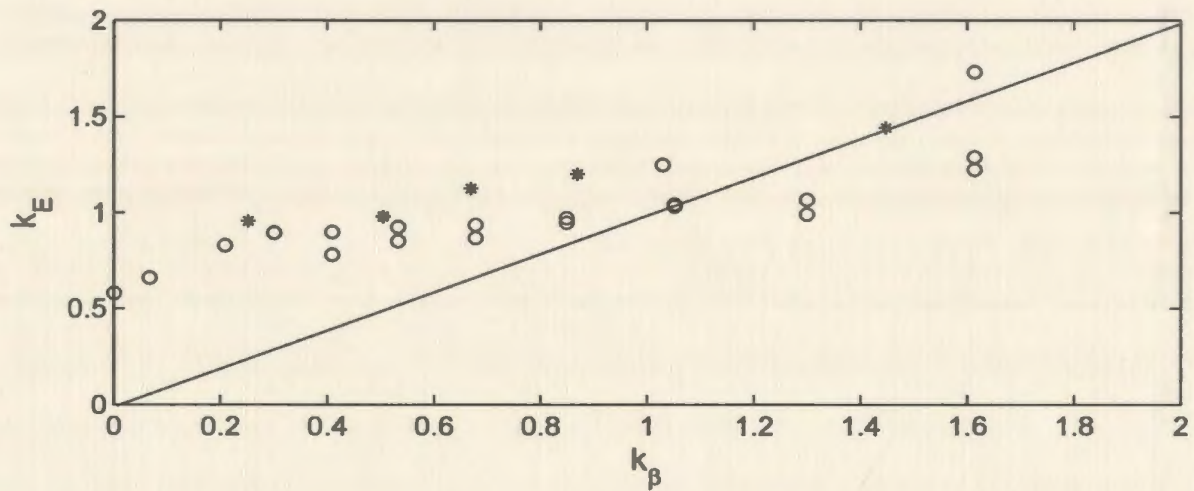


Figure 3.18: Plot of the energy-weighted mean wavenumber k_E versus isotropic Rhines wavenumber k_β : circles - experiments 1- 21 (Table 1), stars - experiments 22- 26.

then decrease rapidly to another constant value after the forcing is stopped. This is consistent with theory in that for non-rotating turbulence it is predicted that k_E should decrease with time corresponding to an upscale energy transfer. However, in the case of beta-plane turbulence, the upscale energy transfer is halted at some point by the formation of zonal jets which would cause the values of k_E and k_{Zonal} to stay constant at later times in the evolution.

The mean values of k_E after the period of rapid decrease were then measured for all of the experiments and were plotted versus the Rhines wavenumber (Rhines scale) (figure 3.18). Recall that this wavenumber represents an isotropic barrier between waves and turbulence. In our case, its value was found by setting the ratio of frequencies in equation (3.3) to unity, averaging over the values of the azimuthal

wavenumber m and then neglecting the anisotropy by taking $m/R = k$ to obtain

$$k_{\beta} = \left(\frac{\beta}{V_{rms}} \right)^{1/2}. \quad (3.4)$$

Figure 3.18 shows that the values of k_E which were measured in our experiments are close to the corresponding theoretical estimates of k_{β} for the experiments with high values of β . This result is not consistent with predictions since strictly speaking the estimate (equation 3.4) implies a steady flow rather than a decaying one. The values of k_E that are shown as stars in figure 3.18 represent the results of a short series of experiments (22-26 in table 1) in which the depth of the layer was 30% less than that of the rest of the experiments. Due to the reduction in the depth of the layer, the energy decay rate in these flows is significantly higher over the same range of β . The results from this series of experiments are consistent with those found in the other experiments. This indirectly implies that dissipation is not a limiting factor in our experiments since it is obviously the β -effect rather than dissipation that provides the arrest mechanism at small wavenumbers.

3.4 Conclusions

In this chapter, the case of decaying two-dimensional turbulence was extended to a more geophysically relevant situation by reproducing this flow on the beta-plane. The two-dimensional energy spectra for the flow with low values of beta was found to be isotropic since the spectrum lies along the isolines of the one-dimensional wavenumber k . The presence of Rossby waves is apparent however in the anisotropic spectrum for the flow with high values of beta. This spectrum is in general consistent with the isolines of the anisotropic Rhines barrier between the wave-dominated region of

spring above the Northern Hemisphere.

Chapter 4

References

Afanasyev, Ya. D., and Korabel, V. N., “Starting vortex dipoles in a viscous fluid: asymptotic theory, numerical simulations, laboratory experiments”, *Phys. Fluids* **16**, 3850 (2004).

Afanasyev, Ya. D., and Wells, J., “Quasi-two-dimensional turbulence on the polar beta-plane: laboratory experiments”, *Geophys. Astrophys. Fluid Dynamics* (2004) accepted.

Arfken, G. B. and Weber, H. J., *Mathematical Methods for Physicists, 5th edition*, Harcourt/Academic Press, Burlington, 2001.

Aubert, J., Jung, S. and Swinney, H. L., “Observations of zonal flow created by potential vorticity mixing in a rotating fluid”, *Geophysical Research Letters* **29**, 1876, doi:10.1029/2002GL015422 (2002).

Bastin, M. E. and Read, P. L., “Experiments on the structure of baroclinic waves and

zonal jets in an internally heated, rotating, cylinder of fluid", *Phys. Fluids* **10**, 374 (1998).

Batchelor, G. K., "Computation of the energy spectrum in homogeneous two-dimensional turbulence", *Phys. Fluids Suppl. II* **12**, 233 (1969).

Batchelor, G. K., *An Introduction to Fluid Dynamics*, Cambridge University Press, New York, 2000.

Beizaie, M. and Garib, M., "Fundamentals of a liquid (soap) film tunnel" *Experiments in Fluids* **23**, 130 (1997).

Boer, G. J., "Homogeneous and isotropic turbulence on the sphere", *J. Atmos. Sci.* **40**, 154 (1983).

Botha, A., "Pictures of the planet Saturn", retrieved from the World Wide Web on July 8, 2004 from <http://www.the-planet-saturn.com/saturn-pictures.html>.

Brachet, M. E., Meneguzzi, M. and Sulem, P. L., "Small-Scale Dynamics of High-Reynolds-Number Two-Dimensional Turbulence", *Phys. Rev. Lett.* **57**, 683 (1986).

Brachet, M. E., Meneguzzi, M. and Sulem, P. L., "The dynamics of freely decaying two-dimensional turbulence", *J. Fluid Mech.* **194**, 333 (1988).

Cardoso, O., Marteau, D. and Tabeling, P. "Quantitative experimental study of the free decay of quasi-two-dimensional turbulence." *Phys. Rev. E.* **49**, 454 (1994).

Carnevale, G. F., McWilliams, J. C., Pomeau, Y., Weiss, J. B. and Young, W. R. "Evolution of vortex statistics in two-dimensional turbulence." *Phys. Rev. Lett.* **66**, 2735 (1991).

Charney, J. G., and DeVore, J. G., "Multiple flow equilibria in the atmosphere and blocking", *J. Atmos. Sci.* **36**, 1205 (1979).

Chasnov, J. R., "On the decay of two-dimensional homogeneous turbulence", *Phys. Fluids* **9**, 171 (1997).

Cheng, X., and Wallace, J. M., "Cluster analysis of the Northern Hemisphere winter-time 500-hpa height field: Spatial patterns", *J. Atmos. Sci.* **50**, 2674 (1993).

Cho, J. Y.-K. and Polvani, L. M., "The emergence of jets and vortices in freely evolving, shallow-water turbulence on a sphere", *Phys. Fluids* **8**, 1531 (1996).

Clercx, H. J. H. and Nielsen, A. H. "Vortex statistics for turbulence in a container with rigid boundaries." *Phys. Rev. Lett.* **85**, 752 (2000).

Couder, Y. J., "Two-dimensional grid turbulence in a liquid film" *Phys. Lett.* **45**, 353 (1984).

Couder, Y., Chomaz, J.M., and Rabaud, M., "On the Hydrodynamics of Soap Films" *Physica D* **37**, 225 (1986).

Cushman-Roisin, B., *Introduction to Geophysical Fluid Dynamics*, Prentice Hall, En-

glewood Cliffs, New Jersey, 1994.

Danilov, S., Dolzhanskii, F. V., Dovzhenko, V. A. and Krymov, V. A., "Experiments on free decay of quasi-two-dimensional turbulent flows", *Phys. Rev. E* **65**, 036316-1 (2002).

Danilov, S. D. and Gurarie, D., "Quasi-two-dimensional turbulence", *Physics - Uspekhi* **43**, 863 (2000).

Danilov, S. and Gurarie, D., "Rhines scale and spectra of the β -plane turbulence with bottom drag", *Phys. Rev. E* **65**, 067301 (2002).

deVerdiere, C., "Quasi-geostrophic turbulence in a rotating homogeneous fluid", *Geophys. Astrophys. Fluid Dyn.* **15**, 213 (1980).

Dole, R. M., and Gordon, N. M., "Persistent anomalies of the extratropical northern hemisphere wintertime circulation: Geographical distribution and regional persistence characteristics", *Mon. Weather Rev.* **111**, 1567 (1983).

Durst, R., Melling, A., and Whitelaw, J. H., *Principles and Practice of Laser Doppler Anemometry*, 2nd Ed. Academic, New York, 1981.

Fincham, A. and Spedding, G., "Low cost, high resolution DPIV for measurement of turbulent fluid flow", *Exps. Fluids* **23**, 449 (1997).

Gharib, M., and Derango, P., "A liquid film (soap film) tunnel to study two-dimensional

laminar and turbulent shear flows" *Physica D* **37**, 406 (1989).

Gibson, C. H., "Turbulence in the ocean, atmosphere, galaxy, and universe", *Appl. Mech. Rev.* **49**, 299 (1996).

Hansen, A. E., Marteau, D. and Tabeling, P. "Two-dimensional turbulence and dispersion in a freely decaying system." *Phys. Rev. E.* **58**, 7261 (1998).

Hide, R., "On source-sink flows stratified in a rotating annulus," *J. Fluid Mech.* **32**, 737 (1968).

Hide, R. and Mason, P. J., "Sloping convection in a rotating fluid", *Adv. Phys* **24**, 47 (1975).

Holloway, G., "Contrary roles of planetary wave propagation in atmospheric predictability", in G. Holloway and B. J. West, eds., *Predictability of Fluid Motions*(American Institute of Physics, New York, 1984), 593-599.

Huang, H. P. and Robinson, W. A., "Two-dimensional turbulence and persistent zonal jets in a global barotropic model", *J. Atmos. Sci* **55**, 611 (1998).

Ingersoll, A. P., Dowling, T. E., Gierasch, P. J., Orton, G. S., Read, P. L., Sanchez-Lavega, A., Showman, A. P., Simon-Miller, A. A. and Vasavada, A. R., "Dynamics of Jupiter's atmosphere", In F. Bagenal, W. McKinnon and T. Dowling, Eds., *Jupiter: The Planet, Satellites and Magnetosphere*, (Cambridge University Press, 2004). preprint available on the World Wide Web at

<http://www.lpl.arizona.edu/showman/publications.html>

Karkoschka, E., "Hubble finds many bright clouds on Uranus", retrieved from the World Wide Web on July 8, 2004 from

<http://hubblesite.org/newscenter/newsdesk/archive/releases/1998/35/image/a>.

Kellay, H., Wu, X., and Goldburg, W., "Experiments with turbulent soap films" *Phys. Rev. Lett.* **74**, 3875 (1995).

Kloosterziel, R. C. and vanHeijst, G. J. F., "An experimental study of unstable barotropic vortices in a rotating fluid", *J. Fluid Mech.* **223**, 1-24 (1991).

Kloosterziel, R. C. and van Heijst, G. J. F., "The evolution of stable barotropic vortices in a rotating free-surface fluid", *J. Fluid Mech.* **239**, 607 (1992).

Kolmogorov, A. N., "The local structure of turbulence in an incompressible fluid for very large Reynolds numbers", *Dokl. Akad. Nauk* **30**, 301 (1941).

Kraichnan, R. H., "Inertial ranges in two-dimensional turbulence", *Phys. Fluids* **10**, 1417 (1967).

Kundu, P. K. and Cohen, I. M., *Fluid Mechanics, 2nd Ed.*, Academic Press, San Diego, 2002.

Lau, N.-C., and Nath, M. J., "Frequency dependence of the structure and temporal development of wintertime tropospheric fluctuationscomparison of a GCM simulation

with observations", *Mon. Weather Rev.*, **115**, 251 (1987).

Lesieur, M., *Turbulence in Fluids*, Kluwer, Dordrecht, 1991.

Lilly, D. K., "Numerical simulation study of two-dimensional turbulence", *Geophys. Astrophys. Fluid Dyn.* **3**, 289 (1972).

Maas, L. R., "Nonlinear and free-surface effects on the spin-down of barotropic axisymmetric vortices", *J. Fluid Mech.* **246**, 117 (1993).

Maassen, S. R., "Self-organization of confined two-dimensional flows", PhD thesis, Eindhoven University of Technology, The Netherlands (2000).

Maassen, S. R., Clercx, H. J. H., and van Heijst, G. J. F., "Decaying Quasi-2D Turbulence in a Stratified Fluid With Circular Boundaries", *Europhys. Lett.* **46** (3), 339 (1999).

Manfroi, A. J. and Young, W. R., "Slow evolution of zonal jets on the beta plane", *J. Atmos. Sci.* **56**, 784 (1999).

Marteau, D., Cardoso, O. and Tabeling, P., "Equilibrium states of two-dimensional turbulence: An experimental study", *Phys. Rev. E* **51**, 5124 (1995).

Martin, B. K., Wu, X. L., Goldberg, W. I. and Rutgers, M. A., "Spectra of decaying turbulence in a soap film", *Phys. Rev. Lett.* **80**, 3964 (1998).

McWilliams, J. C., "The emergence of isolated coherent vortices in turbulent flow", *J. Fluid Mech.* **146**, 21 (1984).

McWilliams, J. C., "The vortices of Two-dimensional turbulence" *J. Fluid Mech.* **219**, 361 (1990).

McWilliams, J. C. and Weiss, J. B., "Anisotropic geophysical vortices", *CHAOS* **4**, 2 (1994).

Montgomery, M. T. and Kallenbach, R. J., "A theory for vortex Rossby-waves and its application to spiral bands and intensity changes in hurricanes", *Q. J. R. Meteorol. Soc.* **123**, 435 (1997).

Montgomery, M. T. and Lu, C., "Free waves on barotropic vortices. Part I: Eigenmode structure", *J. Atmos. Sci.* **54**, 1868 (1997).

NASA/JPL-Caltech, "Full disk neptune", retrieved from the World Wide Web on July 8, 2004 from <http://pds.jpl.nasa.gov/planets/captions/neptune/fullnep.htm>.

Nezlin, M.V. and Snezhkin, E. N., *Rossby Vortices, Spiral Structure, Solitons*, Springer-Verlag, Berlin, Heidelberg, 1993.

Norton, W. A., "Breaking rossby waves in a model stratosphere diagnosed by a vortex-following coordinate system and a technique for advecting material contours", *J. Atmos. Sci.* **51**, 654 (1993).

Nozawa, T. and Yoden, S., "Spectral anisotropy in forced two-dimensional turbulence on a rotating sphere", *Phys. Fluids* **9**, 3834 (1997).

O'Connor, J. F., "The weather and circulation of January 1963: One of the most severe months on record in the United States and Europe", *Mon. Weather Rev.* **91**, 209 (1963).

Paret, J., Marteau, D., Paireau, O. and Tabeling, P., "Are flows electromagnetically forced in thin stratified layers two dimensional?", *Phys. Fluids* **9**, 3102 (1997).

Pawlak, G. and Armi, L., "Vortex dynamics in a spatially accelerating shear layer", *J. Fluid Mech.* **376**, 1 (1998).

Poulsen, C., "Global atmospheric circulation: consequences of a spinning Earth", retrieved from the World Wide Web on July 8, 2004 from <http://earth.usc.edu/geol150/weather/circulation.html>.

Read, P. L., Yamazaki, Y. H., Lewis, S. R., Williams, P. D., Miki-Yamazaki, K., Sommeria, J., Didelle, H. and Fincham, A., "Multiple jet formation in a convectively driven flow on a beta-plane", (XXI ICTAM, 15-21 August 2004, Warsaw, Poland)

Rhines, P. B., "Waves and turbulence on a beta-plane", *J. Fluid Mech.* **69**, 417 (1975).

Rhines, P. B., "Jets", *CHAOS* **4**, 313 (1994).

Rivera, M., Vorobieff, P., and Ecke, R. E., "Turbulence in Flowing Soap Films: Velocity, Vorticity, and Thickness Fields" *Phys Rev. Lett.* **81**, 1417 (1998).

Rutgers, M. A. "Forced 2D Turbulence: experimental evidence of simultaneous inverse energy and forward energy cascades" *Phys. Rev. Lett.* **81**, 2244, (1998).

Rutgers, M. A., "Flowing Soap Films: A Platform for 2D Non-linear Dynamics Experiments" *Nonlinear Science Today*, PII: S09389008 (99) 00001-1 (1999).

Rutgers, M. A., Wu, X. L., and Daniel, W. B., "Conducting fluid dynamics experiments with vertically falling soap films" *Rev. Sci. Inst.* **72**, 3025 (2001).

Salmon, R., *Lectures on Geophysical Fluid Dynamics*, Oxford University Press, New York, 1998.

Santangelo, P., Benzi, R. and Legras, B., "The generation of vortices in high-resolution, two-dimensional decaying turbulence and the influence of initial conditions on the breaking of self-similarity", *Phys. Fluids A* **1**, 1027 (1989).

Scott, R. B., "Evolution of energy and enstrophy containing scales in decaying, two-dimensional turbulence with friction", *Phys. Fluids*, **13**, 2739 (2001).

Sommeria, J., "Experimental study of the two-dimensional inverse energy cascade in a square box," *J. Fluid Mech.* **170**, 139 (1986).

Unisys Weather, "Current Southern Hemispheric 500 mb Plot". Retrieved from the

World Wide Web on

July 30, 2004 from [http://weather.unisys.com/upper_air/ua_shem₅00p.html](http://weather.unisys.com/upper_air/ua_hem500p.html).

Vallis, G. and Maltrud, M. E., "Generation of mean flows and jets on a beta plane and over topography", *J. Phys. Oceanogr.* **23**, 1346 (1993).

Vorobieff, P., Rivera, M. and Ecke, R. E., "Soap Film Flows: Statistics of 2D Turbulence" *Phys. Fluids* **11**, 2167 (1999).

Voropayev, S. I. and Afanasyev, Y. D., "Two-dimensional vortex dipole interactions in a stratified fluid", *J. Fluid Mech.* **236**, 665 (1992).

Voropayev, S. I. and Afanasyev, Y. D., "Vortex quadrupoles and two-dimensional oscillating grid turbulence", *Appl. Sci. Res.* **51**, 475 (1993).

Voropayev, S. I. and Afanasyev, Y. D., *Vortex Structures in a Stratified Fluid*, Chapman and Hall, London, 1994.

Voropayev, S. I., Afanasyev, Y. D. and Filippov, I. A., "Horizontal jets and vortex dipoles in a stratified fluid", *J. Fluid Mech.* **227**, 543 (1991).

Voropayev, S. I., Afanasyev, Y. D., and van Heijst., G. J. F., "Experiments on the evolution of gravitational instability of an overturned, initially stably stratified fluid", *Phys. Fluids A* **5**, 2461 (1993).

Voropayev, S. I., Afanasyev, Y. D., and van Heijst., G. J. F., "Two-dimensional

flows with zero net momentum: evolution of vortex quadrupoles and propagation of turbulent region", *J. Fluid Mech.* **282**, 21 (1995).

Weeks, E. R., Tian, Y., Urbach, J. S., Ide, K., Swinney, H. L. and Ghil, M., "Transitions between blocked and zonal flows in a rotating annulus with topography", *Science* **278**, 1598 (1997).

Wells, J. and Afanasyev, Ya. D., "Decaying quasi-two-dimensional turbulence in a rectangular container: laboratory experiments", *Geophys. Astrophys. Fluid Dyn* **98**, 1 (2004).

Whitehead, J. A., "Mean flow driven by circulation on a β -plane", *Tellus* **27**, 634 (1975).

Wu, X. L., Levine, R., Rutgers, M., Kellay, H., and Goldburg, W. I., "Infrared technique for measuring thickness of a flowing soap film" *Rev. Sci. Inst.* **72**, 2467 (2001).

Yoden, S. and Yamada, M., "A numerical experiment of two-dimensional decaying turbulence on a rotating sphere", *J. Atmos. Sci* **50**, 631 (1993).

1870

1871

1872

1873

1874

1875

1876

1877

1878

1879

1880

